PIEZOELECTRIC MATERIALS AS ENERGY GENERATION DEVICES

BY

Khalid Hayder Abdalla Elkhider

A Thesis Presented to the
DEANSHIP OF GRADUATE STUDIES

KING FAHD UNIVERSITY OF PETROLEUM & MINERALS

DHAHRAN, SAUDI ARABIA

In Partial Fulfillment of the
Requirements for the Degree of

MASTER OF SCIENCE

In

CHEMICAL ENGINEERING

April, 2015

KING FAHD UNIVERSITY OF PETROLEUM & MINERALS

DHAHRAN- 31261, SAUDI ARABIA

DEANSHIP OF GRADUATE STUDIES

This thesis, written by **Khalid Hayder Abdalla Elkhider** under the direction of his thesis advisor and approved by his thesis committee, has been presented and accepted by the Dean of Graduate Studies, in partial fulfillment of the requirements for the degree of **MASTER OF SCIENCE IN CHEMICAL ENGINEERING.**

Dr. Mohammded Ba-Shammakh

Department Chairman

Dr. Abdul-Majeed Azad.

(Advisor)

Dr. Salam A. Zummo

Dean of Graduate Studies

Dr. Mohammed Mozhar Hossain.

(Member)

Dr. Zuhair Omar Malaibari

(Member)

19/5/15

Date

To my parents and my wife with all love

ACKNOWLEDGMENTS

All praise and thanks due to Allah (SWT), who created me, created the chance, and give me the strength and guidance to complete this work. I would like to express my gratitude to my thesis supervisor, Dr. Abdul-Majeed Azad for furnishing me with valuable opinions and guidance on my work.

I am also grateful to thank Dr. Zain H. Yamani, director of Center of Excellence in Nanotechnology, for his valuable advices and his ultimate generosity in supporting this work.

Moreover, I would like to thank the members of thesis committee for their valuable tips and encouragements.

Special thanks to Drs. Mohammad Qamar, Ahsan ul Haq Qurashi, Abbas Hakeem, Mohammed Nasiruzzaman Shaikh, and Md. Abdul Aziz from CENT for materials support.

Thanks also to CENT imaging lab team, Dr. Abbas Hakeem, Mr. Qasem Drmosh, Fatai O. Bakare, Mr. Anas Bin Ali, Mr. Raja M. Awais, Mr. Muhammad Shahzeb, for their patience, dedication, and help during SEM characterization of more than 50 samples.

My gratitude and sincere thanks to Mr. Raashid Muhammad from Physics department for his time and help in the electrical measurements. Also, I would like to thank Dr. Munir Al-Absi, Mr. Felix Doleguez and Mr. Irfan Ahmed (Electrical Engineering Department) for allowing me to use the oscilloscope.

Thanks are due to my colleagues, Mr. Mohammed A. Hassan, Mr. Anas Karrar, Mr. Mohamed Ibrahim, Mr. Khalid Hamid, and to everyone who helped.

My sincere gratitude, love, and respect to my parent, who sacrificed dearly in order for me to become what I am today. Finally, thanks to my wife who, although, came at the last part of this long journey, she had a great hallmarks toward the completion of my degree.

TABLE OF CONTENTS

LIST OF TABLES

LIST OF FIGURES

LIST OF ABBREVIATIONS

DMAc	:	N,N-dimethylacetamide
EHD	:	Energy harvesting device
eV	:	Electron volt
Gr	:	Graphene
HMTA	:	Hexamethylenetetramine
PVDF	:	Polyvinylidene difluoride
V	:	Volt
V_2O_5	:	Vanadium oxide
ZA	:	Zinc acetate
ZN	:	Zinc nitrate
ZnO	:	Zinc oxide

ABSTRACT

Full Name : **Khalid Hayder Abdalla Elkhider**

Thesis Title : Piezoelectric Materials as Energy Generation Devices

Major Field : Chemical Engineering

Date of Degree : April 2015

Ceramic-polymer (*cermer*) composites containing hexagonal ZnO nanorods with 2 wt.% graphene dispersed in polyvinylidene difluoride (PVDF) with or without vanadium oxide (V_2O_5) were prepared by a simple technique using inexpensive starting materials to fabricate energy harvesting devices (EHDs). The effect of using different precursors of zinc, such as, zinc nitrate (ZN) and zinc acetate (ZA), reducing agents (such as urea and Hexamethylenetetramine (HMTA)) and the role of graphene on the particle morphology, yield and, on the performance of EHD was investigated. It was found that in addition to affecting the yield, graphene also assisted in shaping and deagglomeration of ZnO nanorods. Although, ZnO particles synthesized via HMTA-ZA route were thicker and hexagonal in shape, the performance of the corresponding EHD was rather inferior (open circuit voltage under stress ~0.45V). The EHD device fabricated from ZnO obtained via urea-ZN route, on the other hand, showed optimum performance (~25.5V) due possibly to the relatively large aspect ratio of ZnO particles in this case.

The role of V_2O_5 addition to the ZnO/Gr composite was also studied. Addition of 2.5, 5, and 10 wt. % of V_2O_5 appears to affect the ultimate shape and size of the ZnO particles significantly, as compared to those without V_2O_5; systematic transformation from 3D

hexagonal rods to aggregated flower-petals to 2D nanoplatelets was clearly seen. V_2O_5 addition also assisted in enhancing the output voltage of the V_2O_5-modified composites. This was more pronounced in case of ZnO derived from HMTA-ZA route.

ملخص الرسالة

الاسم الكامل:خالد حيدر عبد الله الخضر

عنوان الرسالة: المواد الكهرضغطية كأجهزة لتوليد الطاقة

التخصص: الهندسة الكيمائية

تاريخ الدرجة العلمية: ابريل 2015

من خلال هذا البحث تم بنجاح تحضير مركبة (سيراميك-بوليمر)تتكون من قضبان أكسيد الزنك السداسية نانوية الشكل مع 2% بالوزن من الجرافين وزعت بشكل جيد في بوليمر (PVDF) مع أو بدون أكسيد الفانديوم باستخدام تقنية بسيطة ومواد أولية غير مكلفة نسبيا لصنع أجهزة حصاد الطاقة (EHDs) من خلال تطبيق اجهاد ميكانيكي.تم دراسة تأثير كل من مصدر الزنك (خلات الزنك أو نترات الزنك)، وعوامل التفاعل (اليوريا و HMTA) ودور الجرافين على تشكل الجسيمات والكمية المنتجة من أكسيد الزنك على كفاءة أجهزة حصاد الطاقة. لوحظ أن اضافة الجرافين قد ساعدت بشكل واضح في تشكيل وازالة التكتل من الجسيمات. على الرغم من جودة شكل جزيئات اكسيد الزنك المصنعة بواسطة خلات الزنك و HMTA إلا أن كفاءة جهاز حصاد الطاقة لمقابلة كانت أدنى ما لوحظ (~0.45 فولت) بينما كانت أعلى قيمة سجلت (25.5 فولت) من الجهاز المصمم باستخدام أكسيد الزنك المصنع بواسطة نترات الزنك واليوريا.

تم أيضا دراسة تأثير اضافة أكسيد الفانديوم إلى مركبة أكسيد الزنك/الجرافين (2.5 و 5 و 10% بالوزن من الناتج النظري لأكسيد الزنك)، لوحظ التأثير الواضح على شكل وحجم الجزيئات عند المقارنة مع التي بدونه. لوحظ التحول المنهجي من القضبان سداسية الشكل إلى مجاميع مما يشبه البتلات ثم ما يشبه الصفائح نانوية الشكل. من ناحية أخرى، وجد أن إضافة أكسيد الفانديوم قد ساعدت في تحسين كفاءة جهاز حصاد الطاقة وكان هذا أكثر وضوحا في حالة الجهاز المصمم من أكسيد الزنك المصنع من خلات الزنك و HMTA .

Chapter 1

Introduction

1.1. Thesis motivation

The unprecedented population growth and technological advancements are intimately related to the significant increase in energy consumption. Fossil fuels, such as, coal, oil, and gas are the main sources of energy. They constitute about 86% of the total available energy resources. The increasing energy crisis and the fossil fuel-related global warming has spurred considerable interest in power generation from renewable and green resources, for example, solar power, thermal, wind, ocean and geothermal.

There are ongoing efforts for alternative ways of creating energy, in addition to, from solar or wind which have attained some degree of maturity and commercialization niche. Consequently, new energy resources such as vibration, radiofrequency, thermal, and electromagnetic waves have been identified; they often times are regarded as stray and commonly thought to be waste. Nevertheless, they could be converted into useful electrical energy by energy harvesting devices (EHDs). EHDs refer to autonomous micro/nano energy producing machines. EHDs could make use of thermoelectric generators, micro wind turbine, photovoltaics, and piezoelectric materials, to name a few. One of these devices, namely, the one based on piezoelectric aspects, is the subject of present investigation.

Piezoelectrics are materials that create electricity when subjected to mechanical stress (deformation). They also work in reverse, generating deformation under the influence of an applied electric field. The most common natural piezoelectric material is quartz. Synthetic piezoelectric - mostly ceramics – are, however, more efficient and have been studied in great details for several decades [2-13]. Piezoelectric materials have wide applications ranging from everyday use to more specialized devices (Table 1).

Table 1: Some application areas of piezoelectric materials

Industry	Application
Automotive	Air bag sensor, air flow sensor, audible alarm, fuel atomizer, keyless door entry, seat belt buzzer, knock sensor.
Computer	Disc drives, inkjet printers.
Consumer	Cigarette lighters, depth finders, fish finders, humidifiers, jewelry cleaners, musical instruments, speakers, telephones.
Medical	Disposable patient monitors, fetal heart monitors, ultrasonic imaging.
Military	Depth sounders, guidance systems, hydrophones, sonar.

Figure 1 shows the market forecast for piezoelectric transducers up to 2022 [14]. In recent years, the piezoelectric materials and their composites (such as zinc oxide with polyvinylidene fluoride) have been studied quite extensively, for enhancing the efficiency of such EHDs [2, 4-7, 9-12, 15].

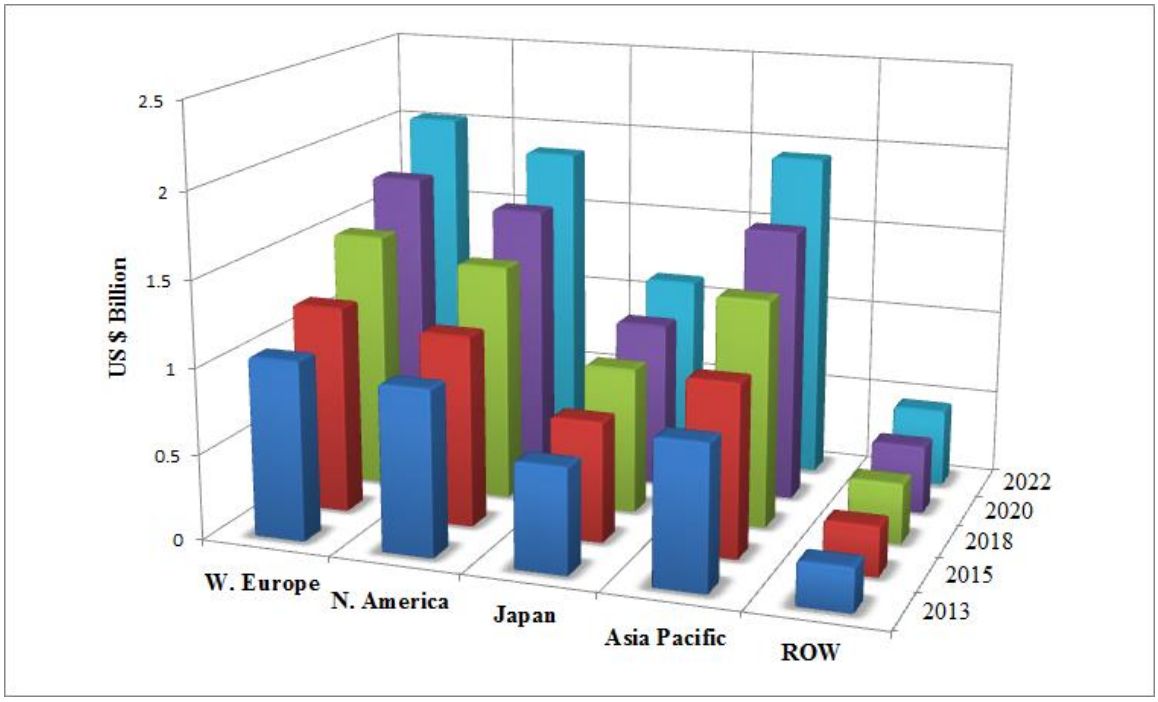

Figure 1: The market forecast for piezoelectric transducers by region [13]

1.2. Objectives

The objective of this work was to fabricate a power generation device consisting of a composite of piezoelectric ceramic (ZnO), nanostructured carbon (graphene) and a polymer (PVDF). The study was focused on the following aspects:

- Use of simple preparative technique and inexpensive starting materials.
- The role of starting precursors, experimental conditions and shape-modifying additives that control and impart exotic morphologies to the main component (ZnO).
- The feasibility of incorporation of other functional materials without compromising the microstructural features and augmenting the performance of the main material.
- Optimization of the synthesis parameters for higher yield.
- Assessment of ZnO-based nanocomposites in terms of EHD performance.

1.3. Thesis overview

The outline of this thesis is as follows. Chapter 2 gives an overview of materials used for fabricating piezoelectric-based EHDs. The review includes history of piezoelectricity and the properties of components used in the present work, viz., ZnO, graphene, V_2O_5 and PVDF. Chapter 3 gives the details of the methodology for making ceramic-polymer nanocomposites from an intimate mixture of 3-D nanoscale ceramic (ZnO), a 2-D nanoscale carbonaceous material (graphene) and a cross-linked polymer (PVDF), with or without V_2O_5. Also included in this chapter are the steps for fabricating the EHD. Chapter 4 deals with the results and discussion on the synthesis of pure ZnO, ZnO with graphene, the influence of precursors, additives, reagents and experimental conditions on the structural and morphological aspects of the resulting materials and their characterization in terms of their energy harvesting response as a function of applied stress. The summary of major findings of this work, conclusions and directions for future work is given in Chapter 5.

Chapter 2

Literature review

2.1. Historical background of piezoelectricity

The word piezoelectricity comes from the Greek word *piezein* meaning *squeeze*; it refers to material's ability to generate electricity under pressure. The piezoelectric effect was first observed and reported by Pierre and Jacques Curie brothers in 1880 [16] in several crystalline materials such as tourmaline, quartz, topaz, cane sugar, and sodium potassium tartrate (Rochelle salt). Quartz and Rochelle salt are natural piezoelectrics displaying most noticeable piezo effect. The Curies did not predict the possibility of reversing piezoelectric effect [17]. Applying mathematics to the fundamental thermodynamics principles, Lipmann proved the existence of reverse piezoelectric effect, which was confirmed by the Curie brothers soon after [18, 19].

The science of piezoelectricity saw a resurgence during WWI, when the French scientist Paul Langevin and his coworkers developed an ultrasonic submarine detector using thin quartz crystals [20]. Their use and the resounding success in sonar opened the floodgates for researchers to look for the development of other piezoelectric devices.

From a fundamental point of view, piezoelectricity is manifested in terms of variation of polarization strength, arising due to: lack of crystal symmetry, orientation of polarization domains within the crystal, and application of mechanical stress. The crystal structure of two most common inorganic piezoelectric materials is shown in Fig. 2.

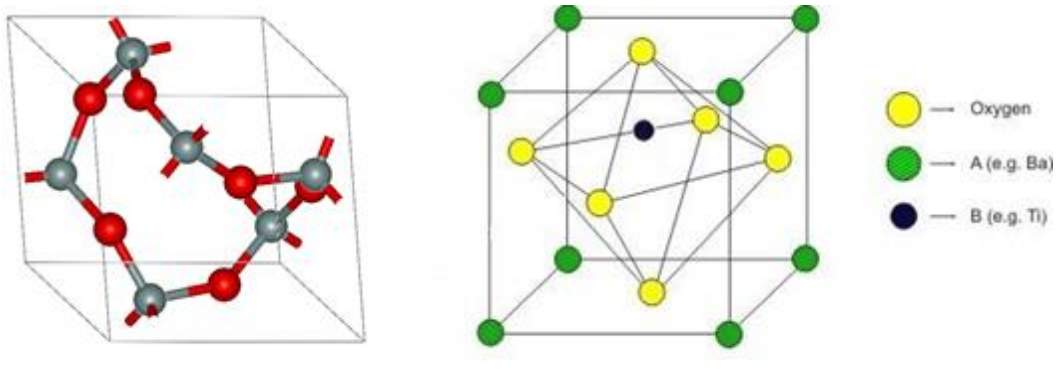

Figure 2: Crystal structures of α-quartz (L), and $BaTiO_3$ (R).

2.2. Zinc Oxide

2.2.1. Zinc oxide and its properties

Zinc oxide (ZnO) is an inorganic compound classified as an n-type semiconducting oxide in the II-VI group. The most attractive properties of ZnO are wide bandgap of ~3.37 eV, high bond energy (60 meV) and, high thermal and mechanical stability at room temperature. Hence, ZnO has the ability to be stable not only during processes at high temperature but also during operations under large electric fields [21]. Due to these distinctive properties, considerable amount of research on ZnO has been carried out in a wide range of scientific fields [7, 22].

The structure of ZnO represents hexagonal crystal system (wurtzite type), as shown in Fig.3. The zinc and oxygen are bonded in a tetrahedron-like arrangement, ZnO_4. The deviation from tetrahedron can be understood in terms of the difference of distance between zinc and oxygen atoms in c direction and that in the Zn-O basal plane. Moreover, the bond length along the c-axis is longer than the other three bonds by about 0.96%; this causes the ZnO_4 tetrahedron to distort along the c-axis, resulting in net dipole moment [23].

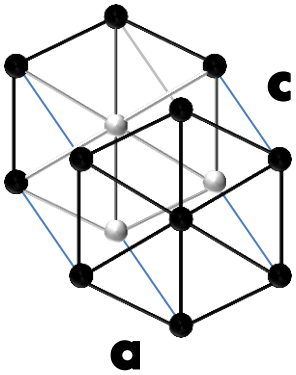

Figure 3: **General schematics of a hexagonal crystal**

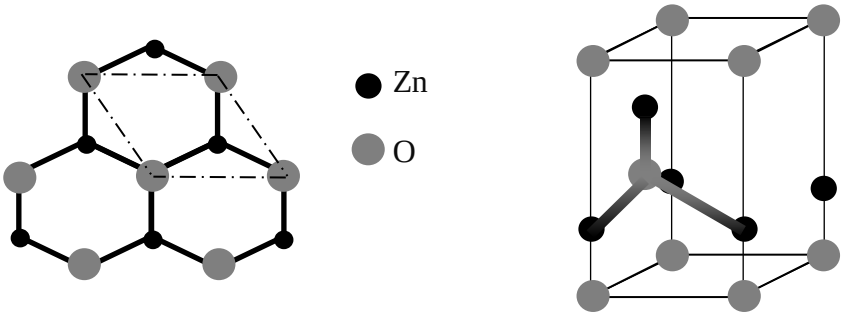

Figure 4: Wurtzite structure of ZnO

2.3. Graphene

Graphene (Gr) is a crystalline allotrope of carbon. Since its discovery in 2004 [24], it has shown unique properties such as high specific surface area, mechanical strength, and electronic conductivity. Due to its sheet-like assembly structure, graphene has a unique band structure, where carbon atoms form hexagonal lattice on a 2-D plane [25]. Graphene is also a semiconductor of ~zero band gap and hence behaves like metal; it is more metallic than the conventional metals. But this is true only for a graphene layer that is just a few nanometers thick. In relevance to the work reported in this thesis, graphene was thought to cause improvement in the electrical conductivity of ZnO [15, 25-27].

2.4. Polyvinylidene fluoride

Polyvinylidene fluoride (PVDF) is a fluorinated thermoplastic polymer with low density compared to other fluoropolymers. Due to its high purity, remarkable strength, resistance to solvents, acids, bases and, heat, it has been used in a large number of applications, such as, ultrasonic transducers, insulation of electrical wires and sensors. Due to its polar crystalline structure, PVDF has excellent piezoelectric properties by itself, compared to other polymeric materials [6]. PVDF consists of at least five different structural forms depending on whether the chain is in trans (T) OR gauche (G) linkage [28]. The most common PVDF varieties are identified as α- (non-polar) or β- (polar) form.

Although the α-phase exists in large quantities compared to the β-phase, it is the later (β-phase) that is responsible for the piezoelectric response of PVDF.

As can be seen from Fig. 7, β-phase has a higher degree of polarity with oriented hydrogen and fluoride (CH_2–CF_2) unit cells along the carbon backbone. In order to obtain β-PVDF, electrical poling and mechanical stretching processes are required during the manufacturing process to align the dipoles in the crystalline PVDF structures [29, 30].

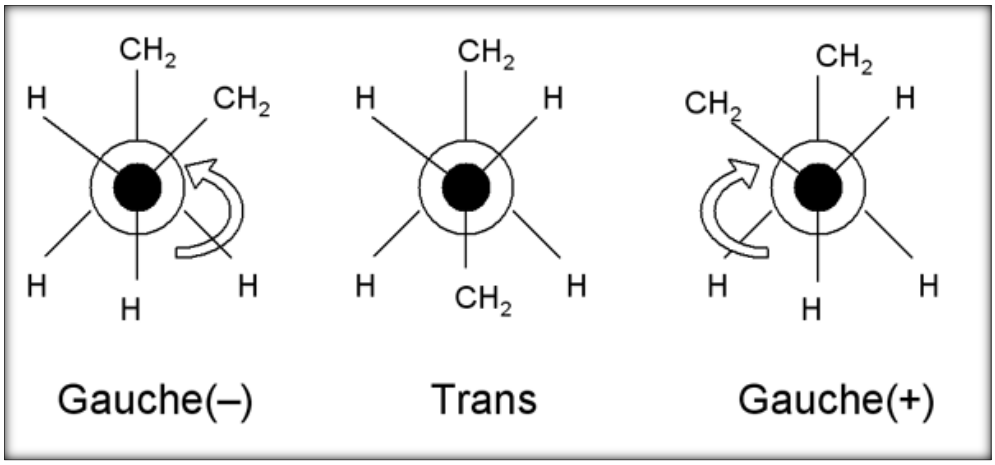

Figure 5: Newman projections conformations of the bonds around each carbon atom[31]

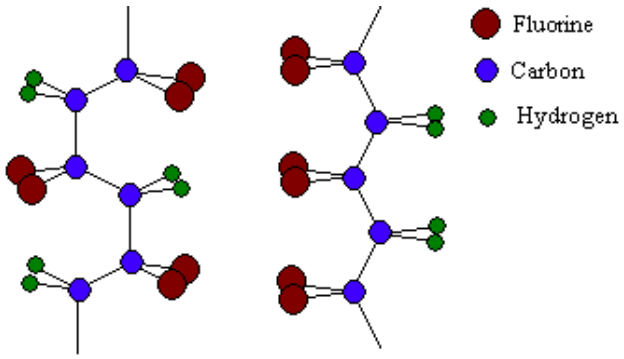

Figure 6: Crystal structure of PVDF: Non-polar α-phase (L) and polar β-phase (R) [1]

2.5. Pure/hybrid ZnO as piezoelectric energy harvesting device

Although the piezoelectricity in ZnO was discovered more than five decades ago [32], its first application as a thin film piezoelectric for the generation/detection of surface acoustic waves (SAW) on non-piezoelectric substrate was investigated only in 1976 [33]. This led to many other applications such as, surface acoustic wave (SAW) resonator, filter, sensor, and micro- and nano-electromechanical systems (MEMS and NEMS).

The first successful attempt to apply piezoelectric concept using nanoscale ZnO was reported by Wang and Song [7]. They measured the voltage generated by the aligned ZnO nanowires grown on alumina substrate. The ZnO array was coated with silver paste to make a continuous conducting surface and a platinum-coated silica tip of an atomic force microscope (AFM) was used in the contact mode. The generated device voltage was ~6-9 mV at the highest peak with external resistivity of 500 MΩ (efficiency 17-30%). This breakthrough led to the possibility of using ZnO nanorods as well for EHDs and, devices with ZnO nanorods arrays (either vertical or lateral) with higher efficiency of a single rod compared to an array have been reported, as they tend to produce higher currents [34]. Fabrication of lighter ZnO-based EHD with more flexibility and cost-effectiveness on plastic substrates has also been widely reported. Voltage up to 350 mV from standard single layer of ZnO nanorods has been generated [35].

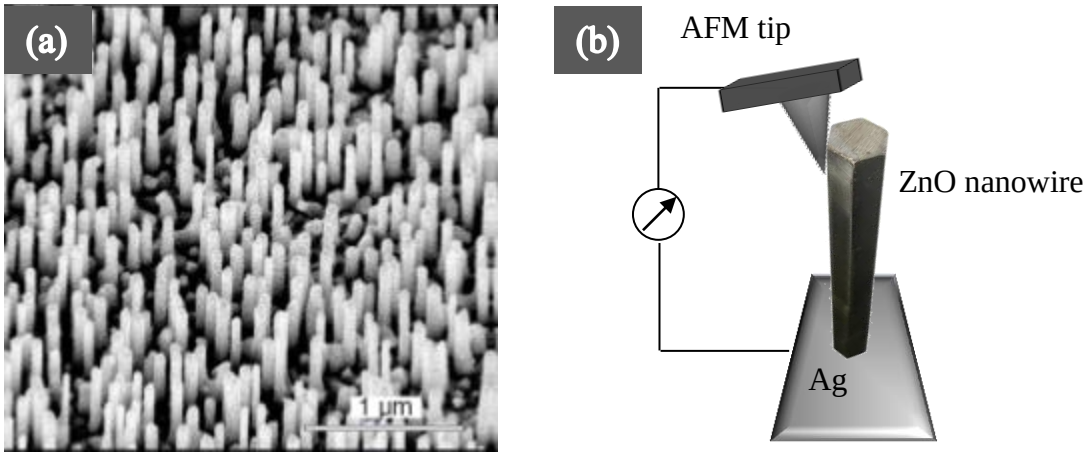

Figure 7: (a) SEM of aligned ZnO NWs growing on Al_2O_3 substrate. (b) Sketch illustrates the AFM-based measurement of the bending-induced piezoelectric potential of ZnO NWs [7].

Zhu et al. [36] increased the efficiency by transferring vertically aligned nanorods to a lateral film with the ability to connect rods in both series and parallel array unlike previous devices, where the contacts were limited to the top and bottom arrays alone.. In this case, a voltage as high as 2V with the current density of 0.1 µA cm^{-2} could be achieved. 10 V was generated by growing an array on both sides of a flexible substrate and covering the array with thin layer of insulating polymer before coating with the top contact [37]. Others have reported the possibility of a hybrid piezoelectric device by compositing ZnO nanorods with PVDF; the electrical outputs were ~0.1 V and ~10 nA cm^{-2} [30]. Table 2 shows some of the ZnO-based piezoelectric materials, its output and applications.

Hence, devices based on ZnO nanorods hold great promise route for fabricating a flexible wearable nanogenerator to harvest piezoelectric potential [6, 8, 30, 37]. In fact, it may be

a suitable alternative to the traditional rigid ceramic-only energy harvesting devices if comparable power densities could be achieved.

Table 2: Some of the ZnO-based piezoelectric materials, its output and applications

Material	Applications	Output (mV)	Ref.
Thin layer ZnO	SAW	--	[33]
Aligned ZnO nanowires	EHD	~6-9	[7]
ZnO/Plastic substrates	Environmental sensor /EHD	350	[35]
ZnO/PVDF	Wearable nanogenerators	~1 x 10^2	[30]
Lateral ZnO nanowire	Light-emitting diode, self-powering	2 x 10^3	[36]
Zn/Au, Ag-coated PVDF	Mechanical deformation by external force	2.4 x 10^3	[38]

Chapter 3

Materials and Experimental Methods

3.1. Materials

The following materials were used as-received in this research, without any purification or additional treatment.

- Zinc nitrate hexahydrate [$Zn(NO_3)_2.6H_2O$] from Fluka Analytical (AR grade, 98+% purity, Switzerland)
- Zinc acetate dihydrate [$Zn(CH_3COO)_2.2H_2O$] from ACS Chemical (AR grade, 98+% purity, India)
- Urea [$CO(NH_2)_2$] from Baker (98+% purity, France)
- Hexamethylenetetramine [$(CH_2)_6N_4$] from Sigma Aldrich (98%+ purity, Germany)
- Graphite flakes (3442, Asbury Graphite Mills, USA)
- Graphene (H-15 grade) from XG Sciences, USA.
- Ammonium metavanadate [NH_4VO_3] from Sigma Aldrich (99.5% purity, USA)
- Polyvinylidene difluoride [$-(C_2H_2F_2)_n-$] (Kynar®, Arkema, France, MW_a: 460,000 Dalton)

3.2. Synthesis of pure/hybrid zinc oxide

Various methods for the synthesis of nanoscale ZnO have been reported in the literature [12, 39-41]. The morphology and the shape of ZnO particles depend on the technique and precursors employed. The most commonly used chemical methods include: precipitation, sol-gel, mechanochemical, organometallic combustion, hydrothermal, solvothermal, etc.

Because of ZnO's multifunctionality, the synthesis methods have been studied extensively. One of the dominant morphologies that can be obtained by different methods is the hexagonal wurtzite structure [39, 40]. The exact shape of the crystal depends on the mechanism of formation in addition to the conditions of synthesis. Different methods create ZnO of unique shapes. Hence, choice of precursors is important. For example, ZnO particles of different shapes and size were fabricated in this work by using urea or hexmethyltetraamine as the reducing agent. The morphology also depends on the nature of the starting precursor and its concentration relative to that of the reducing agent. Moreover, temperature exerts significant effect on the morphology and the product purity. In one case, it was found that the particles formed under sub-boiling conditions were composed of zinc basic carbonate, while those formed under fully boiling conditions were composed of either a mixture of zinc basic carbonate and zinc oxide, or, pure zinc oxide [41].

In the present investigation, a facile and relatively simple homogeneous precipitation method, using urea or hexamethyltetramine as reducing agent and zinc nitrate (ZN) or zinc acetate (ZA) as the zinc precursor, was employed. The aim of using different reducing agents and zinc sources was to understand their role in the evolution of ZnO morphology in terms of particle shape and size. Anticipating an enhancement in the

performance of the ZnO-based EHDs, ZnO nanostructures were grown directly onto graphene due to its unique thermal, electrical and mechanical characteristics, by adding it to the reaction mixture a priori. In order to enhance the performance further, small amounts of vanadium oxide (V_2O_5) were introduced in the ZnO-graphene composite in the form of ammonium meta vanadate (NH_4VO_3). Finally, the ZnO-Gr or ZnO-V_2O_5-Gr formulations were dispersed in 10 wt.% solution of PVFD in acetone and cast into flexible strips by drying at room temperature. The strips were poled and their performance was assessed by monitoring the electrical output signal (in terms of voltage) under different levels of stress stimulus. These measurements were carried out before and after poling the film in order to study the poling effect on the efficiency of the device.

When hexmethyltetramine (HTMA) and zinc nitrate ($Zn(NO_3)_2$) are used, the chemical reactions can be summarized as follows [42]:

a. HMTA hydrolysis:

$$(CH_2)_6N_4 + 6H_2O \rightarrow 6HCHO + 4NH_3 \quad [1]$$

b. Ammonia dissolution:

$$NH_3 + H_2O \leftrightarrow NH_4^+ + OH^- \quad [2]$$

c. Zinc salt ionization

$$Zn(NO_3)_2 \leftrightarrow Zn^{2+} + 2\,NO_3^- \quad [3]$$

Supersaturation reaction:

$$Zn^{2+} + 2OH^{-} \rightarrow Zn(OH)_2 \downarrow \quad [4]$$

ZnO nanorod formation and growth reaction:

$$Zn(OH)_2 \rightarrow ZnO \downarrow + H_2O \quad [5]$$

Formaldehyde formed during the process in reaction [1] reacts with ammonia to form an imine via reductive amination:

$$HCHO + NH_3 \rightarrow CH_2 = NH + H_2O \quad [6]$$

Similarly, zinc acetate ionizes as follow:

$$Zn(COOCH_3)_2 = Zn^{2+} + 2CH_3COO^{-} \quad [7]$$

The formation of net shaped hexagonal nanorods of zinc oxide with hexmethyltetraamine as a reductant is likely due to the presence of iminoethylene as a capping agent.

In the case of urea, all steps are identical to those shown for HMTA, except urea hydrolysis:

$$CO(NH_2)_2 + H_2O \rightarrow CO_2 + 2NH_3 \quad [8]$$

If all of CO_2 is not expelled, a possible side reaction could lead to the formation of zinc basic carbonate or bicarbonate, as follows:

$$2\,Zn^{2+} + CO_2 + 4OH^- \leftrightarrow Zn_2[(CO_3)(OH)_2] + H_2 \qquad [9.a]$$

Or $$Zn^{2+} + 2CO_2 + 2OH^- \leftrightarrow Zn[(HCO_3)_2] \qquad [9.b]$$

Although, by using such reaction schemes, one can control the size, shape, and the purity of the product easily, these techniques, however suffer from the limitations of mass/bulk production on industrial scale, making them economically non-viable.

3.2.1. Standard (Stock) Solution Preparation

In order to synthesize ZnO particles, standard solutions of the precursors, reducing agents, and additives were prepared as follow:

- 0.35 M zinc nitrate hexahydrate (MW = 297.48 g/mol).

  26.0296 g of $Zn(NO_3)_2.6H_2O$ was dissolved in 100 ml deionized water under constant stirring, followed by dilution to 250 ml.

- 0.35 M zinc acetate dihydrate (MW = 219.51 g/mol).

  19.2071 g of $Zn(COOCH_3)_2.2H_2O$ was dissolved in 100 ml deionized water under constant stirring, followed by dilution to 250 ml.

- 4.17 M urea (MW = 60.06 g/mol).

  62.6126 g of $CO(NH_2)_2$ was dissolved in 100 ml deionized water under constant stirring, followed by dilution to 250 ml.

- 0.14 M hexamethylenetetramine (MW = 140.186 g/mol).

  4.9065 g of HMTA was dissolved in 100 ml deionized water under constant stirring, followed by dilution to 250 ml.

3.2.2. Synthesis of pure ZnO using urea

In a typical synthesis, 10 ml of 4.17 M urea solution was diluted with 230 ml of DI water and heated to boiling under reflux condition in a 500mL round bottom flask. It was boiled for 20 min, at which point 10 ml of 0.35 M zinc nitrate (ZN) or zinc acetate (ZA) solution was added and the mixture boiled further for additional 15 min. The molarity of urea and zinc precursor in the final solution was 0.17 M and 0.014 M, respectively. The precipitate was separated from the solution by centrifugation, washed first with water several times and then with acetone, and dried in an air oven at 110°C overnight.

3.2.3. Synthesis of pure ZnO using HMTA

The procedure for making ZnO with HMTA was similar to that described above with urea. In this case, 10 ml of 0.14 M HMTA solution was diluted with 90 ml of DI water and heated to boiling under reflux in a 500mL round bottom flask. It was boiled for 20 min, at which point 10 ml of 0.35 M ZN or ZA solution was added and the mixture boiled further for additional 15 min. The molarity of HMTA and zinc precursor in the final solution was 0.013 M and 0.034 M, respectively. The precipitate was separated from the solution by centrifugation, washed first with water several times and then with acetone, and dried in an air oven at 110°C overnight.

3.2.4. Synthesis of ZnO/graphene composite

Due to its unique thermal, electrical and mechanical characteristics and to examine if it imparts benign effect to the final EHD, graphene was incorporated in the reaction mixture by adding it to the refluxing solution in the amount of 2, 5 and 15 wt.%, relative to the theoretical amount of ZnO obtained in each of subsection 3.2.2 and 3.2.3. In this case, the

equivalent amount of graphene turned out to be 5, 10 and 50 mg, respectively. All other synthesis parameters were kept constant.

3.2.5. Synthesis of V_2O_5-ZnO/graphene using HMTA

It had been reported that the presence of vanadium (as V_2O_5) can augment the performance of ZnO-based piezoelectric nanodevices [12, 42, 43]. The weight percent of vanadium pentoxide (V_2O_5) was varied systematically from 2.5 and 5 wt.% to 10 wt.% and its effect on the morphological variation of ZnO nanostructure and on the performance of resulting EHDs was studied; vanadium was added via solution route for homogeneous distribution throughout the matrix, in the form of ammonium metavanadate (NH_4VO_3). For this, the amount of NH_4VO_3 was computed so as to yield composites whose composition was 2.5 wt.% V_2O_5-(ZnO/Gr), 5 w.t% V_2O_5-(ZnO/Gr) and 10 wt.% V_2O_5-(ZnO/Gr). In a typical synthesis, 10 ml of 0.14 M HMTA with 5 mg of graphene was diluted with 90 ml of DI water and heated to boiling under reflux in a 500 mL round bottom flask. After boiling the mixture for 20 min, 10 ml of 0.35 M ZN (or ZA) solution and 1.9 ml, 3.8 ml or 7.6 ml of 0.041 M NH_4VO_3 (so as to give 2.5, 5 and 10 wt.% of V_2O_5, respectively, in the final product) were added and the mixture boiled for additional 15 min. The precipitates were separated by centrifugation, washed first with water several times and then with acetone. They were dried in an air oven at 110°C overnight and calcined at 450°C for 1h.

3.3. Fabrication of ZnO-based energy harvesting device

ZnO-based EHD was fabricated by mixing ZnO/graphene powder (with or without V_2O_5) with PVDF solution followed by natural curing at the ambient temperature. For this purpose, PVDF solution was prepared by dissolving 10 g of solid PVDF powder in 100 ml acetone under constant stirring at 50°C; this yielded a 10 wt. % PVDF solution in acetone. For making flexible films, 0.1, 0.2 or 0.4 g of ZnO/graphene powder were individually added to 10 ml of 10% wt. PVDF and mixed under vigorous stirring for 1h. Finally, the solution was poured in a cylindrical mold and left to dry naturally for 2 h.

3.3.1. Poling of the ceramic-polymer composite film

Poling was performed in order to align the piezoelectric domains within the materials by applying high voltage (~200V/cm) across it. Under normal conditions, in an unpoled macroscopic piezoelectric specimen the dipoles are randomly oriented with the net polarization becoming zero. Thus, in a sample with randomly oriented dipoles the piezoelectric effect will be negligible. Therefore, it is important to induce an initial state in the material where most of the dipoles are oriented in one direction. When such a sample experiences stress or deformation, it would respond by giving out an electrical stimulus. Such an ordering is achieved by poling the specimen. The direction along which the dipoles align is known as the *poling direction*.

Poling was done by placing the cermer composite specimen between two thin stainless-steel plates, each attached with electrically conducting wires. A high voltage source (Canberra, model 3002) and a digital multimeter DMM (Fluke, model 87) were

connected in series and the other leads were attached to the two plates completing the circuit. The DMM was used to monitor the leakage current.

Chapter 4

Results and discussion

4.1. XRD Characterization

The samples were characterized by XRD (Miniflex, Rigaku diffractometer) using Cu K_α radiation (1.5405 Å) for phase identification and to confirm the crystallinity. Dual beam field-emission scanning electron microscope (LYRA3 Tescan) equipped with energy dispersive X-ray spectrometer (EDX, Oxford Instruments), and transmission electron microscope (JEM-2100F) were utilized to investigate the morphological and microstructural aspects. Phase evolution and thermal stability of the product were ascertained by themrogravimetric analysis using TGA1 (Mettler Toledo).

4.1.1. Pure ZnO

a. From ZN and urea

The XRD pattern (2-θ range: 25–80°; scanning step: 0.02°) of ZnO powder prepared by refluxing aqueous solutions of urea and zinc nitrate (ZN) as per the procedure described in section 3.2.2 is shown in Figure 8. All the diffraction peaks matched with those of single phase hexagonal ZnO conforming to the standard ICCD card no. 01-080-0074. No additional peaks associated with any impurity phase were found.

b. ZA and urea precursors

ZnO was also prepared using zinc acetate (ZA) and urea, as described in section 3.2.2, and its XRD signature is also included in Figure 8. As can be readily seen, the two patterns are identical.

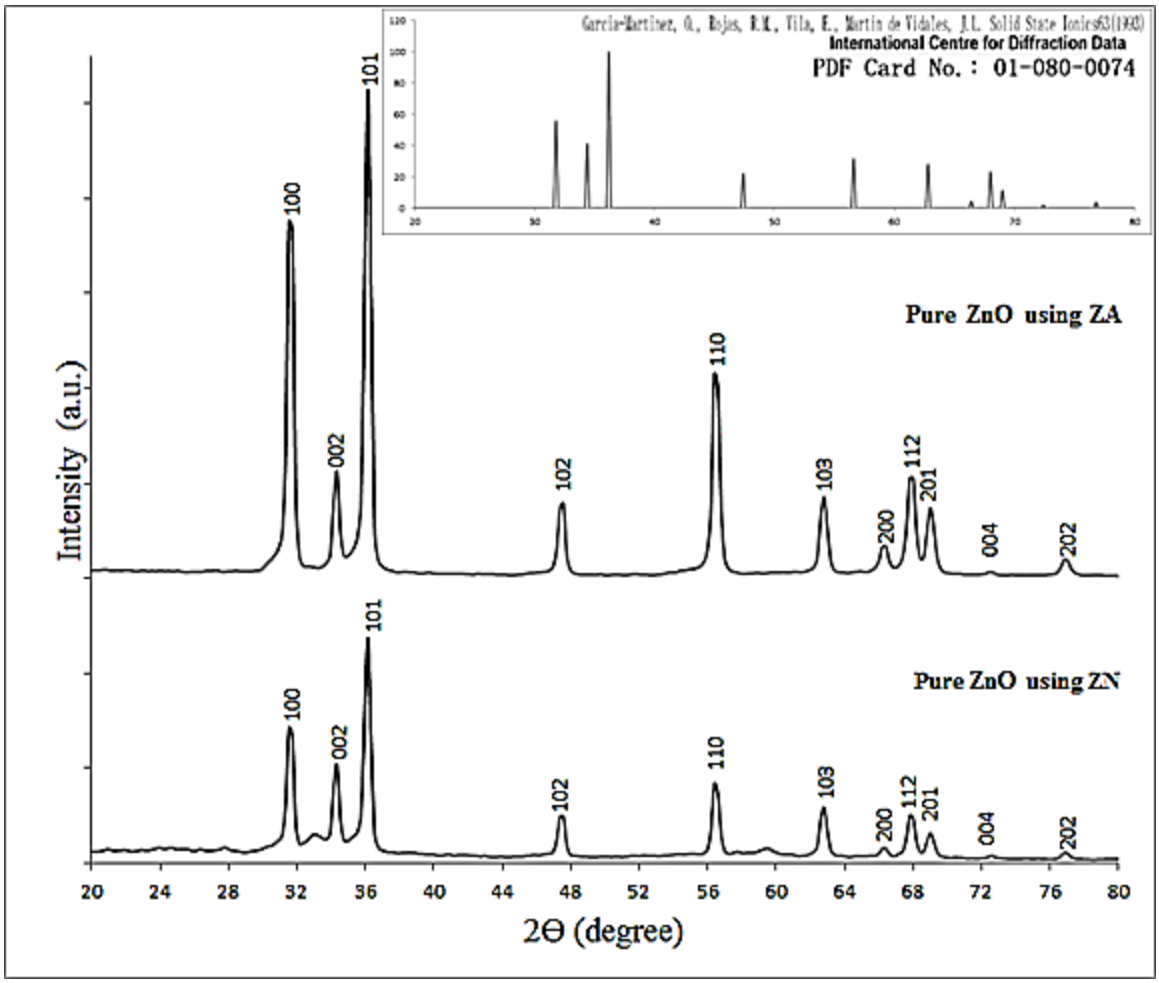

Figure 8: XRD patterns of ZnO prepared from urea and ZA and ZN precursors

c. ZN and HMTA precursors

The XRD pattern of phase pure and highly crystalline ZnO synthesized by refluxing aqueous solutions of zinc nitrate and HMTA (Section 3.2.3) is shown in Figure 8.

d. ZA and HMTA precursors

The XRD pattern of phase pure and highly crystalline ZnO synthesized by refluxing aqueous solutions of zinc acetate is shown in Figure 9; as seen, both the patterns match that of hexagonal wurtzite (ICCD card no. 01-080-0074).

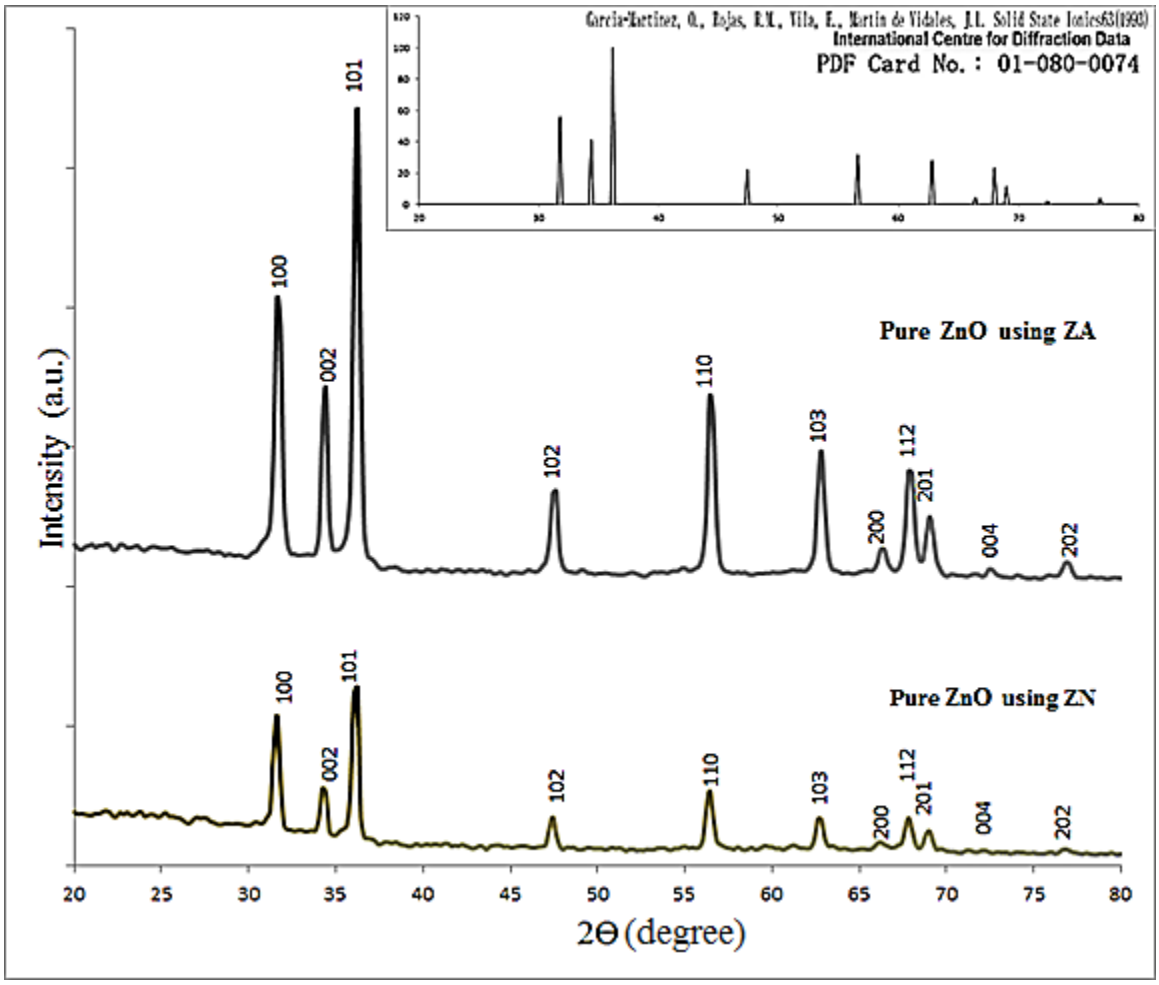

Figure 9: XRD patterns of ZnO prepared from HMTA and ZA and ZN precursors

4.1.2. Microstructural evolution in pure ZnO

1. Urea - ZN/ZA route

Figure 10 shows FE-SEM images of ZnO synthesized via urea route. Images (a) and (b) are for ZnO particles synthesized using urea-ZN and urea-ZA precursor, respectively. These images clearly show that the aspect ratio of ZnO is higher in the case of ZN precursor than that when ZA was used. This could partly be attributed to different modes of Zn^{2+} release in the two cases. Zinc nitrate being a simple molecule is likely to decompose in aqueous media, in a single step creating free Zn (II) ions, which then react with urea (and its decomposition products, as illustrated in Eqs. 1 through 9) to form ZnO in a facile way where nucleation and growth occur simultaneously. In the case of ZA, however, creation of Zn (II) ions occurs through the acetate-to-carbonate path, which is not necessarily synchronous. This leads to formation and nucleation followed by somewhat delayed growth of ZnO particles in the case of ZA. This hypothesis is further strengthened by the fact that the ZnO particles synthesized from ZA are more organized and well-defined in shape (rods with sharp hexagonal edges; Figure 10b). Moreover, in the latter case, ZnO particles are smaller, implying larger surface area compare to those synthesized from ZN.

It can be clearly seen that in both the cases, urea yields agglomerated particles, more noticeably when ZA is used as the zinc source. This could be due to small particle size, large surface area and hence, relatively large surface energy – all favoring agglomeration in order to minimize the surface energy.

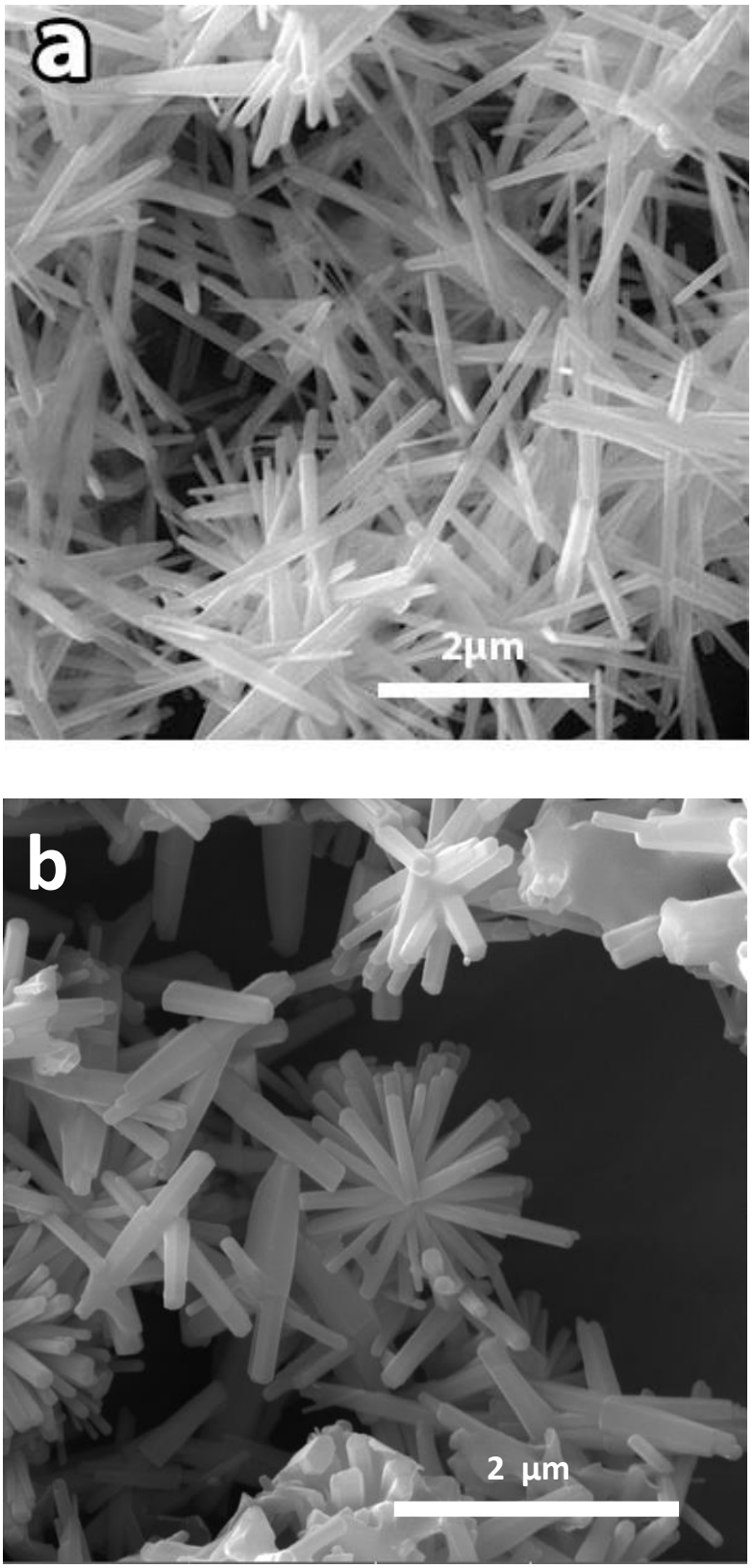

Figure 10: Morphology of ZnO particles synthesized at 110°C via homogeneous precipitation method using urea and: (a) ZN and (b) ZA

2. HMTA - ZN/ZA route

The morphological features of ZnO made with HMTA as the reducing agent and ZN or ZA are zinc source, are shown in Figure 11. Unlike the distinctly difference morphological features of urea-derived ZnO with different zinc precursors (Fig. 10) , the morphology (hexagonal rods) of the HMTA-derived ZnO particles was identical, irrespective of the zinc precursor used; the most interesting difference in this case is perhaps the fact that ZnO rods obtained with ZA are thicker and more well-defined in shape with sharp hexagonal edges. However, in this case as well, the aspect ratio of ZnO obtained from ZN is larger than that from ZA, which bears the same explanation as that given above. In terms of the effect of reducing agent itself higher degree of agglomeration is seen in the case of HMTA compared to urea, but the particle size is much smaller with both Zn and ZA precursors, which could be attributed to the relatively large surface area and high surface energy of smaller particles in the case of HMTA-derived ZnO.

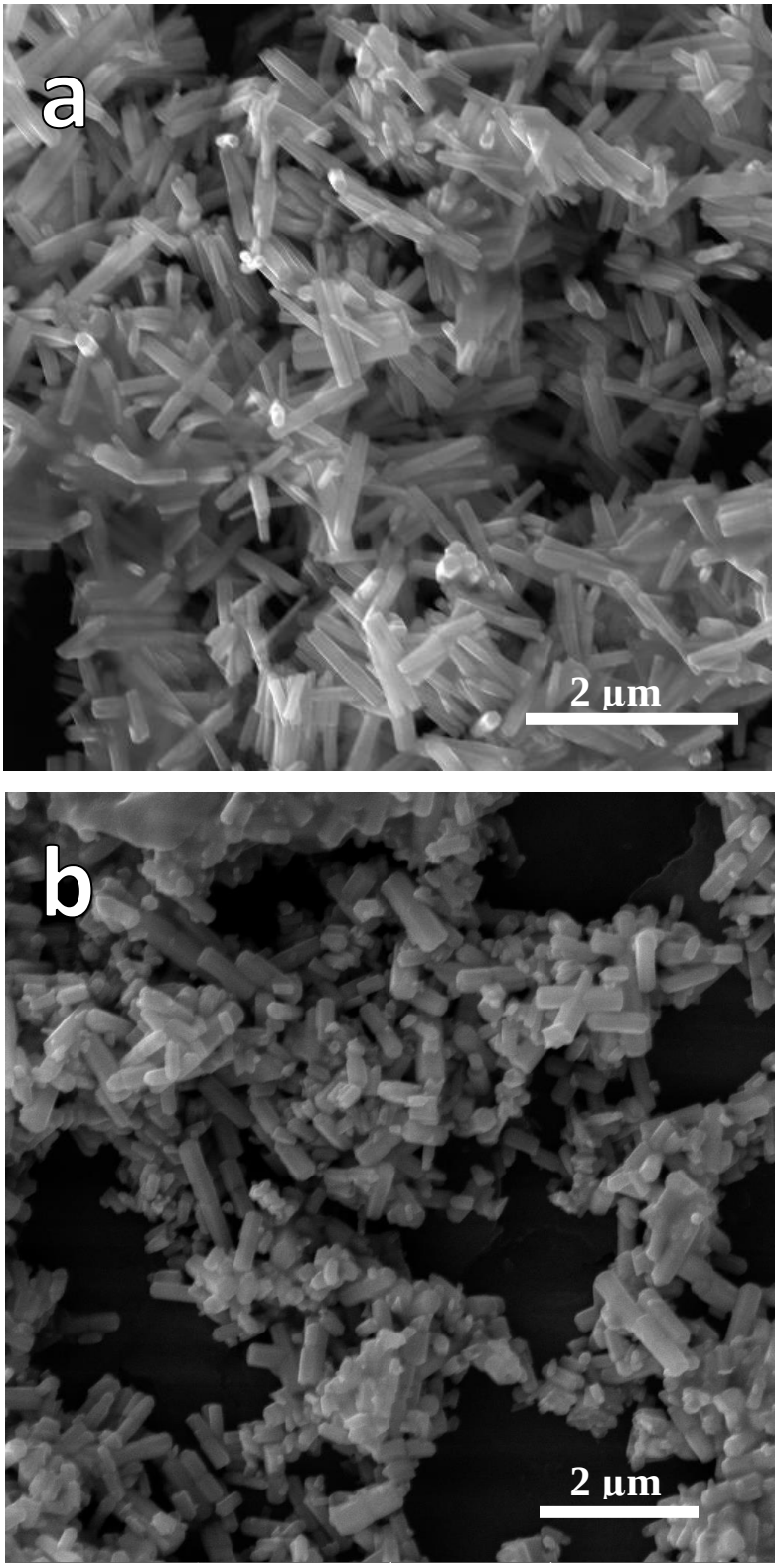

Figure 11: Morphology of ZnO particles synthesized at 110°C via homogeneous precipitation method using HMTA and: (a) ZN and (b) ZA

4.1.3. Comparison of the structural and microstructural features of ZnO from different zinc sources

In terms of phase purity and crystallinity, there was no difference in ZnO made either with urea or HMTA using ZN or ZA (Figs. 8 and 9). The crystallite size of the ZnO particles in the two cases is summarized in Table 3,as calculated by applying Scherer's equation to the (101) reflection:

$$\tau = \frac{K\lambda}{\beta cos\theta}$$

Where:

τ: is the mean size of the crystallites (nm)

K: Shape factor (0.9)

β: Full width at half maximum intensity FWHM (radian)

λ: X-ray wave length (in this case, 0.15405 nm)

Table 3: Mean crystallite size of ZnO particles made with different reactants

	λ/nm	**FWHM/°**	**β/rad**	**2- θ/°**	**θ/rad**	**cosθ**	**τ/nm**
Urea + ZN	0.15405	0.3918	0.006839087	36.1471	0.3155	0.95	21.32
Urea + ZA	0.15405	0.4165	0.007270239	36	0.3142	0.95	20.05
HMTA + ZN	0.15405	0.3899	0.006805921	36.132	0.3154	0.95	21.42
HMTA + ZA	0.15405	0.3471	0.006058823	36.0927	0.3150	0.95	24.06

The characteristic dimensions as estimated from respective FE-SEM images (Figure 12) of ZnO particles are summarized in Table 4. As it can be seen, the average size of ZnO particles synthesized via HMTA route is generally smaller than those from urea, which results in aspect ratio for HMTA-derived particles smaller than that of the urea-counterparts. Furthermore, irrespective of the reductant used, the aspect ratio of particles made with ZN precursor is approximately 2.5-3 times larger than that using ZA.

Table 4: Comparison of aspect ratios of ZnO particles made with urea and HMTA as reductant and ZN or ZA as precursor

	Urea		HMTA	
	ZN	ZA	ZN	ZA
Average length (μm)	1.7	0.72	0.9	0.54
Average width (μm)	0.27	0.27	0.25	0.44
Aspect ratio (l/d)	6.3	2.7	3.6	1.2

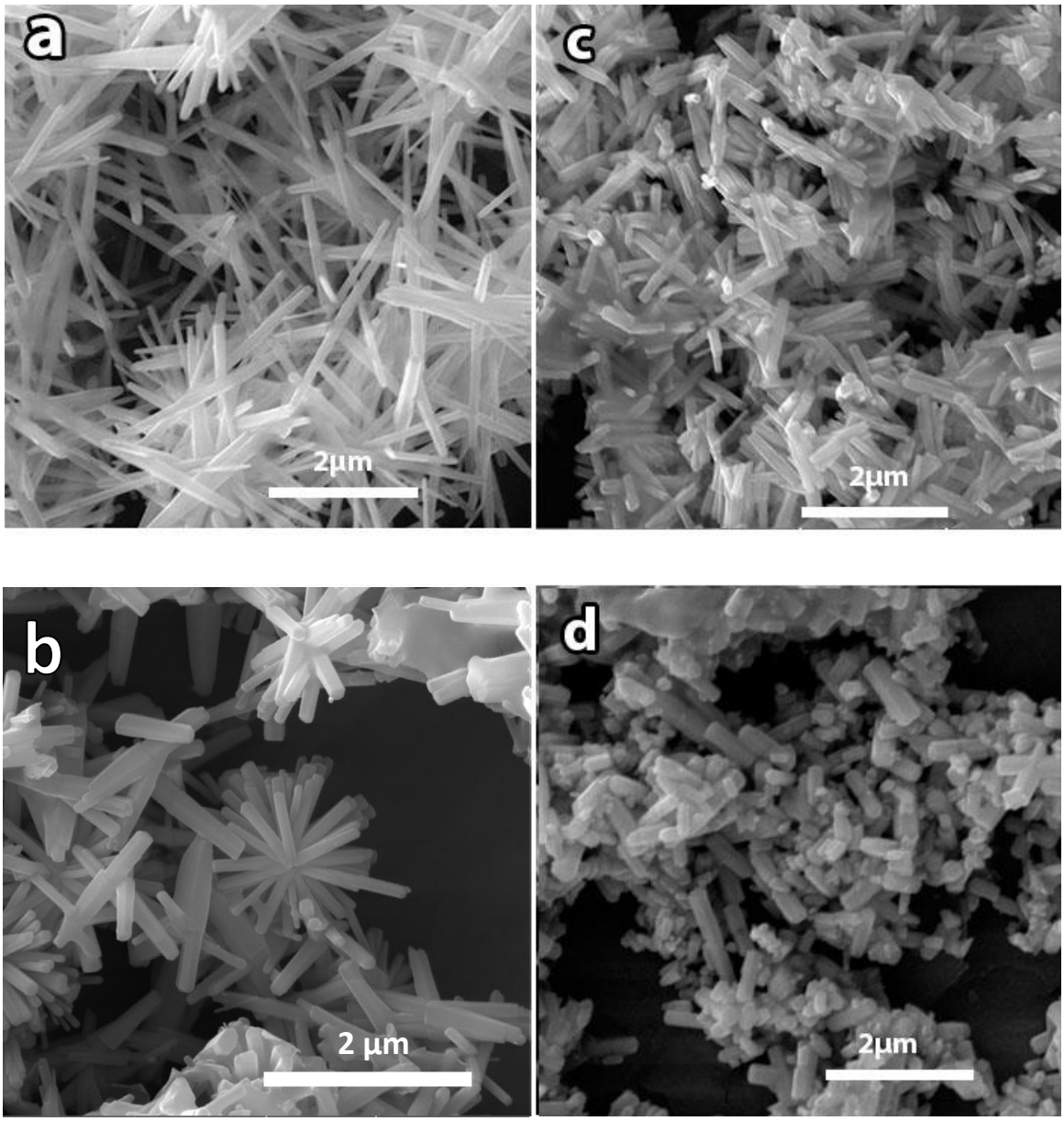

Figure 12: FE-SEM images of ZnO synthesized using: (a) urea-Zn, (b) urea-ZA, (c) HMTA-Zn and (d) HMTA-ZA

4.2. ZnO/graphene composite

4.2.1. XRD Characterization

a. ZnO from Urea - ZN/ZA precursors

The XRD patterns of ZnO powder prepared by refluxing aqueous solutions of urea and zinc nitrate (ZN) or zinc acetate (ZA), in the presence of graphene (15 wt.% of ZnO) are shown in Figure 13. All the diffraction peaks conformed to those of ZnO (ICCD card no. 01-080-0074); the peak at 2-θ = 26.26 is due to graphene (ICCD card no. 00-041-1487). No impurity peaks were found.

b. HMTA - ZN/ZA precursors

The XRD patterns (Figure 14) of the ZnO/graphene composites were identical to those presented in Figure 13.

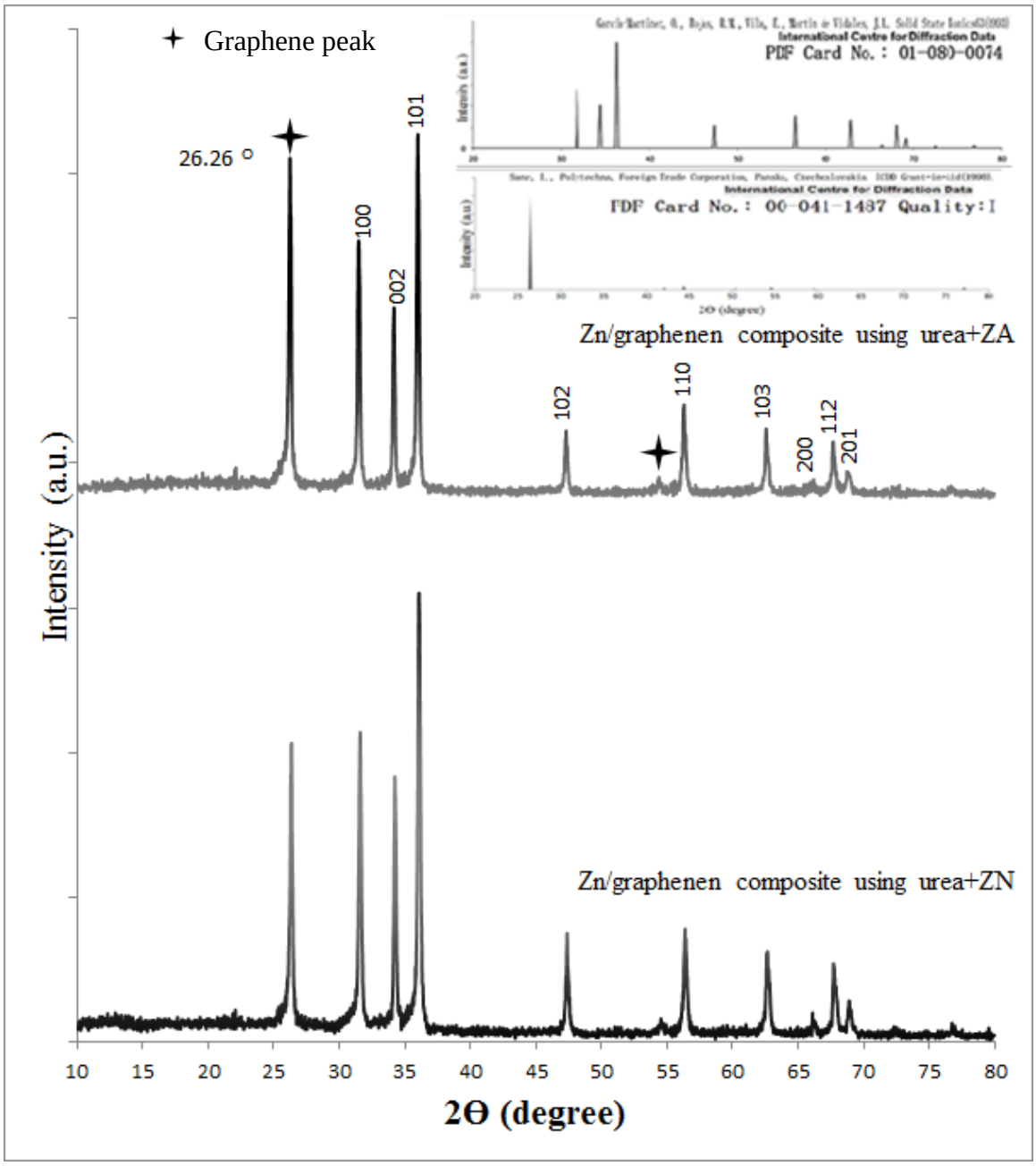

Figure 13: XRD patterns of ZnO prepared from urea and ZA and ZN precursors with 15 wt.% graphene

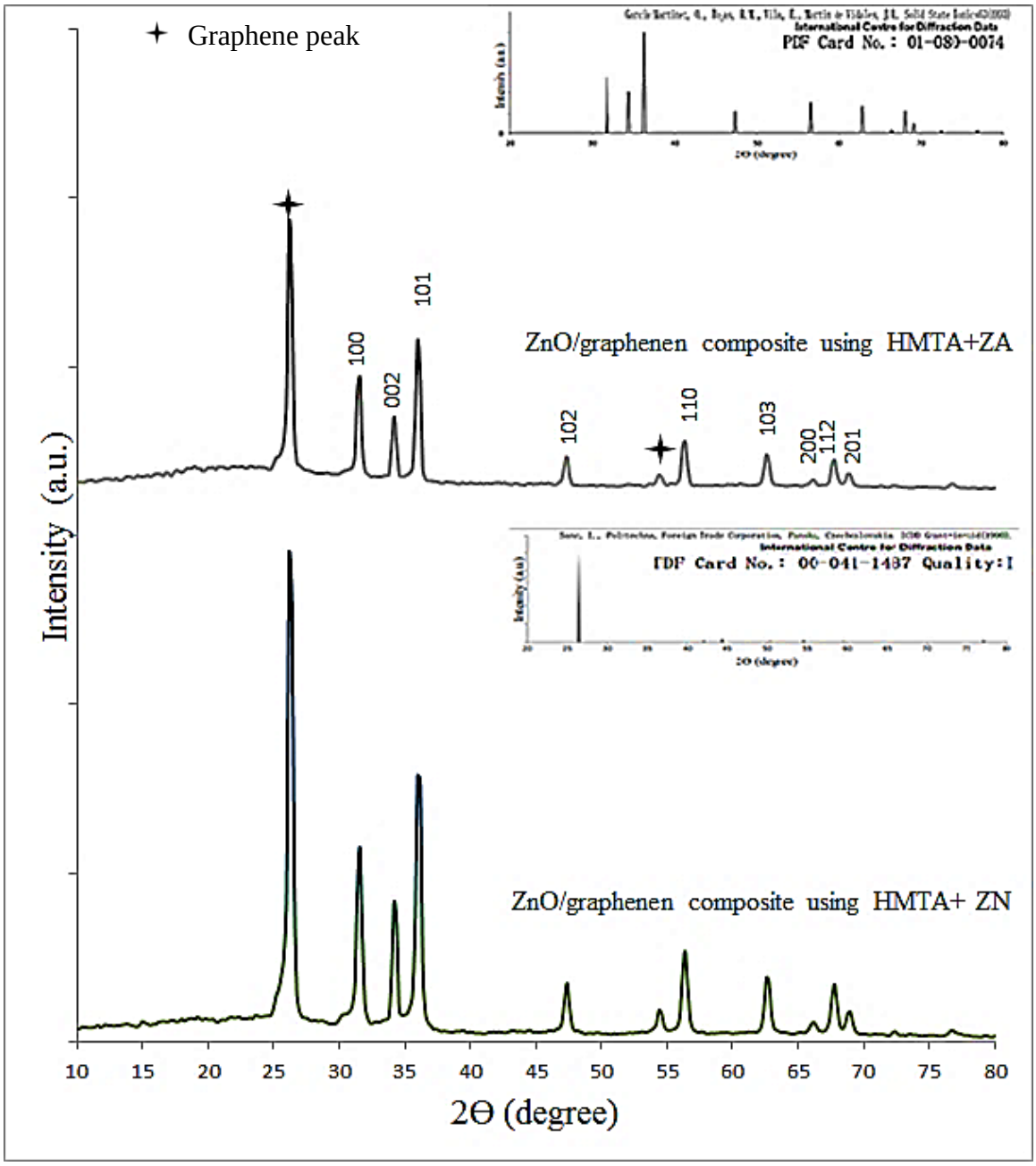

Figure 14: XRD patterns of ZnO prepared from HMTA and ZA and ZN precursors with 15 wt.% graphene

4.2.2. Microstructural characterization

1. ZnO (urea – ZN)/graphene composite

The morphology of the ZnO particles made in the presence of graphene is shown in Figure 15. As can be clearly seen, the effect of systematic addition of graphene on the resulting morphology of ZnO in the composites is interesting. In general, particles are of hexagonal rod shape, irrespective of the amount of graphene in the composite. Also, there is evidence of several ZnO rods growing normal to the graphene surface. Clearly, the incorporation of graphene appears to have significantly influenced the size distribution and degree of agglomeration in addition to imparting individuality and sharpness to shape of the particles which appear as well-shaped hexagonal rods with well-defined edges. Interestingly, the presence of graphene also appears to have aided in increasing the yield: the amount of ZnO produced appears to be higher compared to that without graphene. Moreover, the ZnO yield is higher when less amount of graphene is used. Thus, some catalytic and shape-modifying/controlling aspect of graphene is operative. It is worth pointing out for the sake of comparison, that ZnO particles derived from urea-ZN route were predominantly needle-like with large aspect ratio. The aspect ratio of ZnO formed in the presence of graphene is summarized in Table 5. Interestingly, while the particle width remained almost invariant (~0.13 μm), there was a small but systematic increase in the length with graphene content. For ready comparison, data for pure ZnO particles (wt.% graphene = 0) are also included.

Table 5: Variation of aspect ratio of ZnO particles in the urea-ZN derived ZnO/graphene composite

	Amount of graphene (wt.%) in the composites			
	0	**2**	**5**	**15**
Average length (μm)	1.7	0.96	1.07	1.58
Average width (μm)	0.27	0.14	0.11	0.13
Aspect ratio	6.3	6.86	9.73	12.15

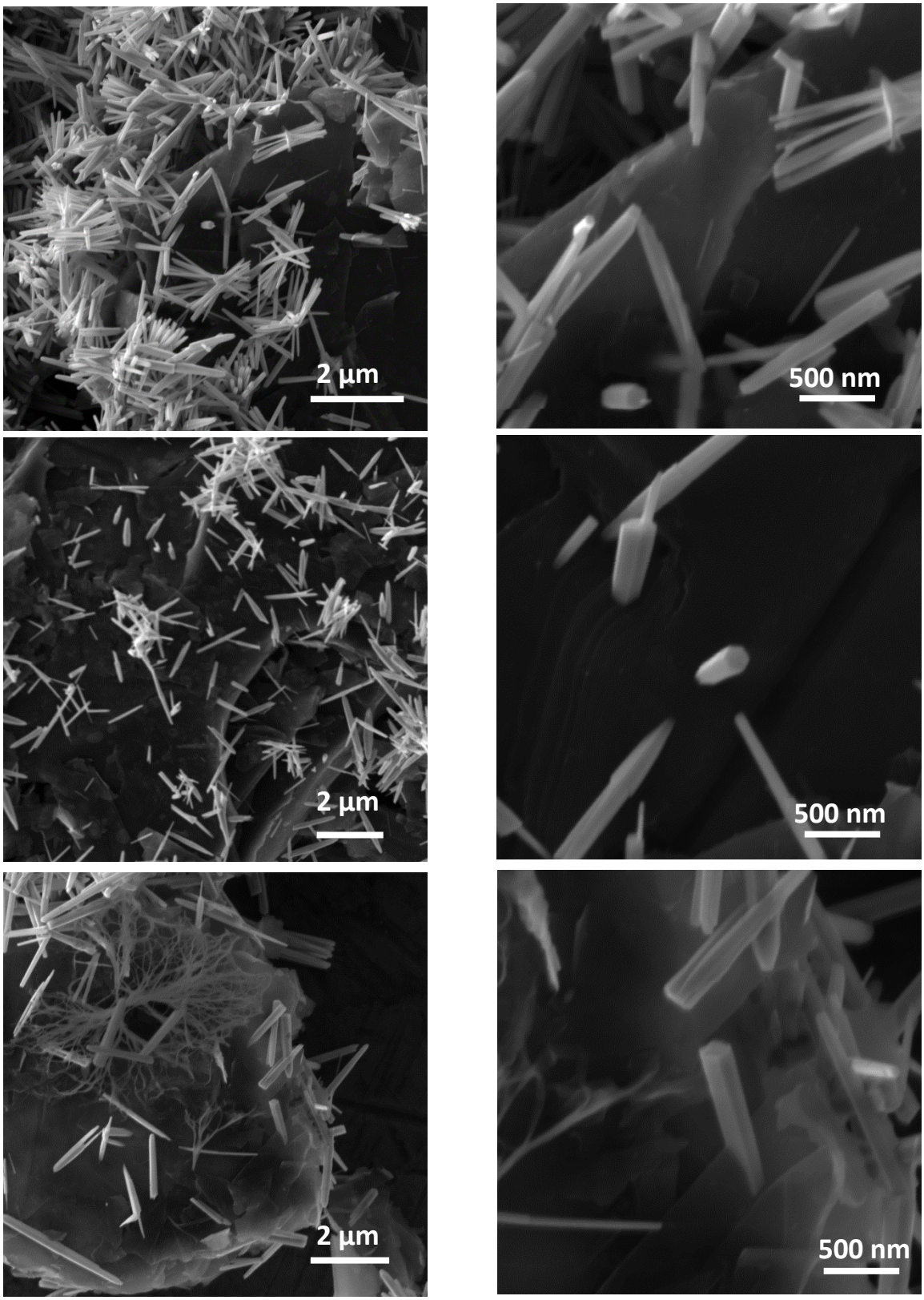

Figure 15: SEM images of ZnO/graphene composites synthesized via urea-ZN route containing: (top) 2 wt.% (center) 5 wt.% and (bottom) 15 wt.% of graphene.

2. ZnO (urea – ZA)/graphene composite

Figure 16 shows the SEM images of much smaller but well-defined, individual hexagonal ZnO particles (synthesized by urea and ZA) in the composites. Clearly, using ZA as zinc precursor yielded thicker and shorter well-defined hexagonal rods; the dependence of particle size and aspect ratio variation on the graphene content is shown in Figure 17. As explained above in the case of pure ZnO formation, these differences could be attributed to the difference in decomposition pathways of ZA as opposed to ZN as a precursor; ZA takes more time to decompose and hence contributes to slow nucleation and growth of ZnO particles. In addition to higher yield, formation of hollow hexagonal ZnO rods is visible in the case of lowest graphene content. In the case of nucleation and growth of tubular ZnO, one of the common mechanisms/hypotheses [44-50] proposes selective etching of ZnO along the c axis in the (001) plane by high concentration of H^+ or OH^- in solution [44-50].

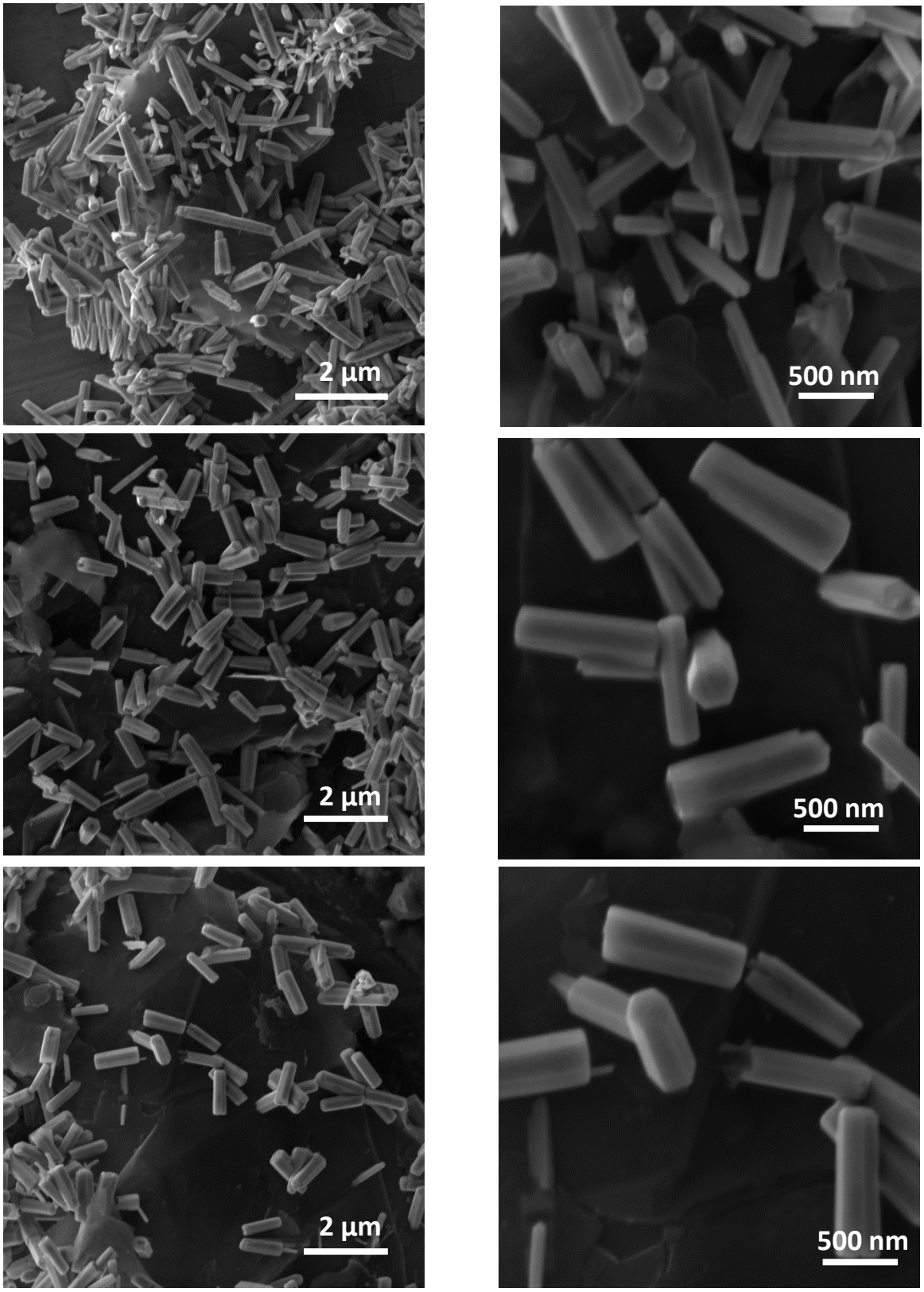

Figure 16: SEM images of ZnO/graphene composites synthesized via urea-ZA route containing: (top) 2 wt.%, (center) 5 wt.% and (bottom) 15 wt.% of graphene.

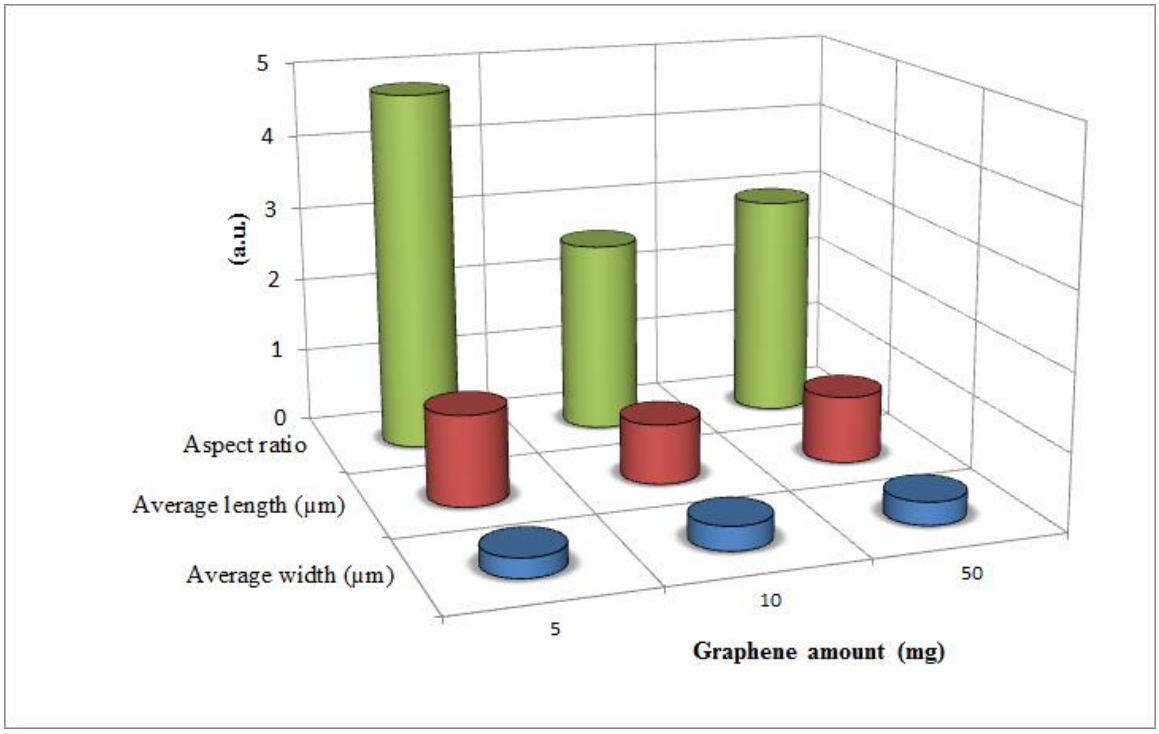

Figure 17: Variation of aspect ratio of ZnO particles in the urea-ZA derived ZnO/graphene composite

3. *ZnO(HMTA –ZN)/graphene composite*

In this case, hexagonal ZnO rods were formed uniformly with some of them growing vertically on the graphene surface, as shown in Figure 18. In this case as well, it is evident that graphene plays a decisive role towards the shape, size and yield of the ZnO particles. Also, the yield is higher with the lowest level of graphene. The rod length increases proportionately with increasing amount of graphene in the composite, while the rod thickness practically remains invariant. This is summarized in Figure 19.

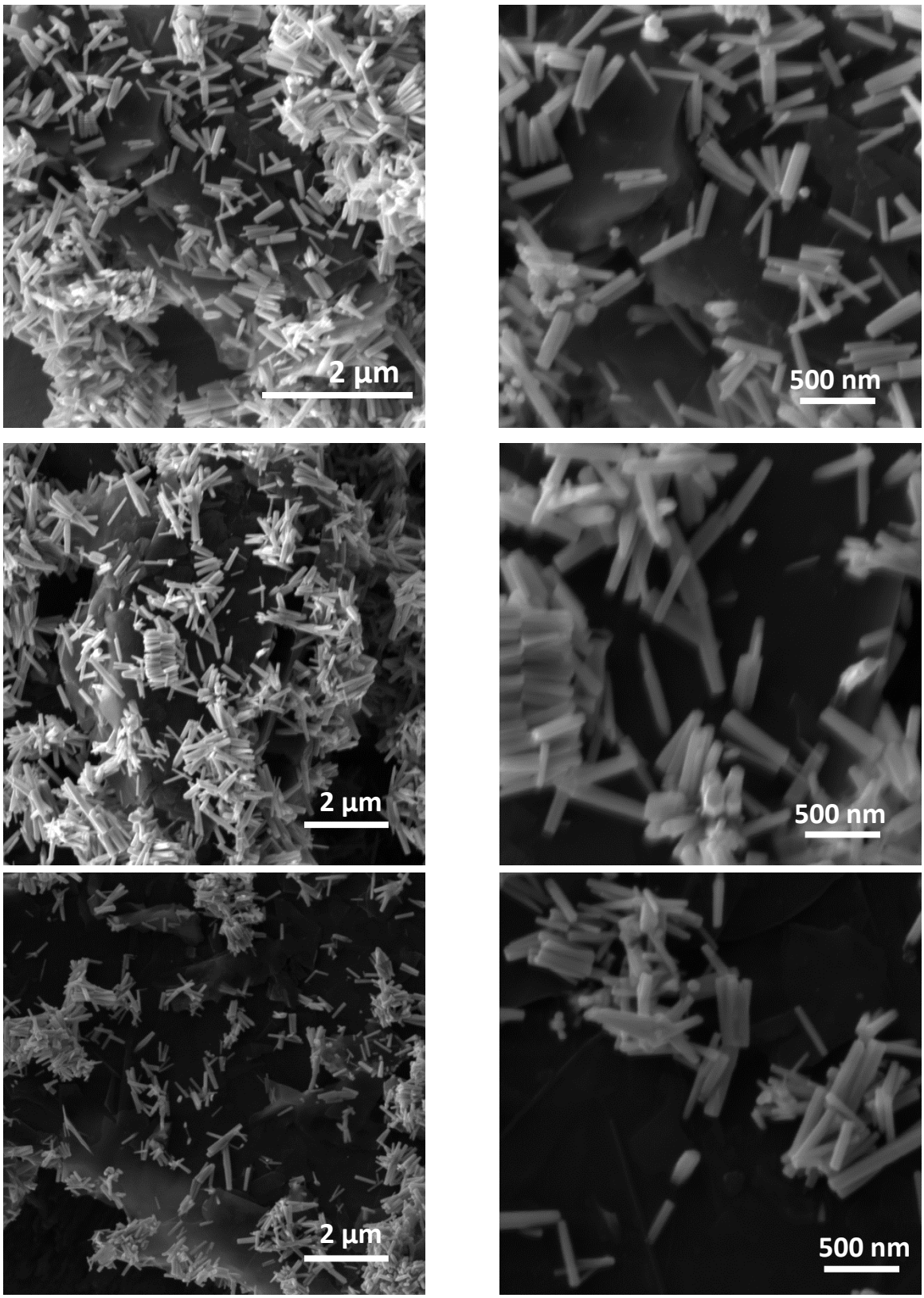

Figure 18: SEM images of ZnO/graphene composites synthesized via HMTA-ZN route containing: (top) 2 wt.%, (center) 5 wt.% and (bottom) 15 wt.% of graphene.

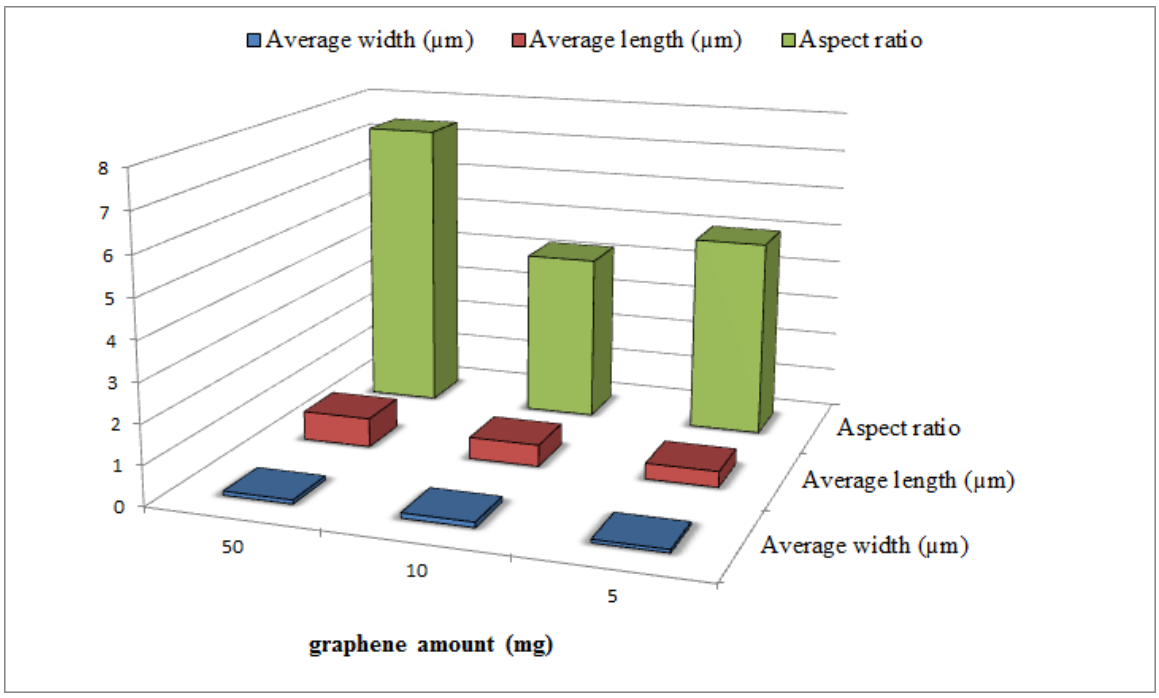

Figure 19: Variation of aspect ratio of ZnO particles in the HMTA-ZN derived ZnO/graphene composite

4. ZnO(HMTA - ZA)/graphene composite

In this case, very short, thick but well-separated hexagonal rods formed as shown in Figure 20; formation of hollow ZnO nanorods was also observed. The average particle sizes and variation of aspect ratio are summarized in Table 6. For ready comparison, data for pure ZnO particles (wt.% graphene = 0) are also included.

Table 6: Variation of aspect ratio of ZnO particles in the HMTA-ZA derived ZnO/graphene composites

	Amount of graphene (wt.%) in the composites			
	0	**2**	**5**	**15**
Average length (μm)	0.9	0.44	0.38	0.34
Average width (μm)	0.25	0.3	0.22	0.25
Aspect ratio	3.6	1.47	1.73	1.36

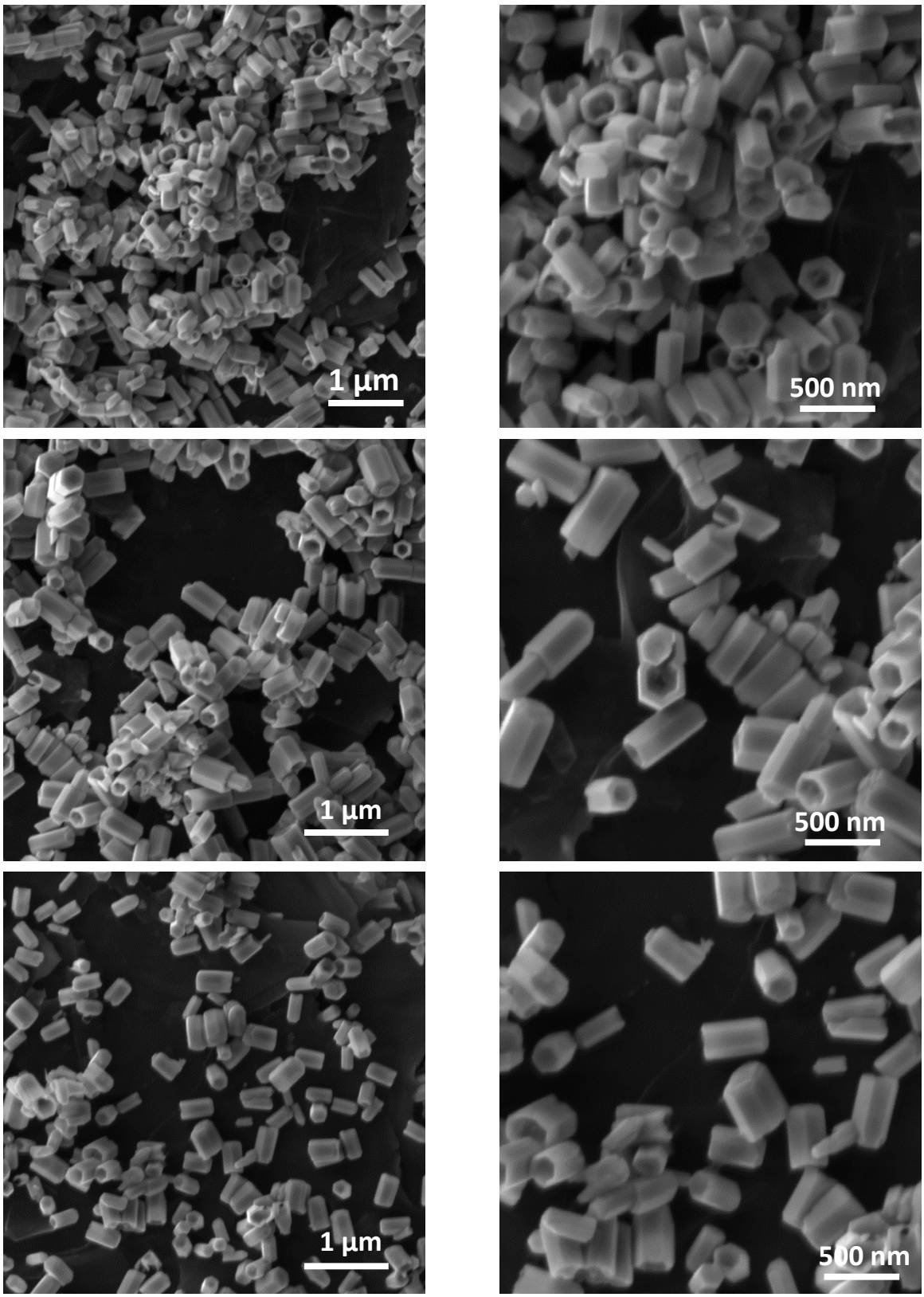

Figure 20: SEM images of ZnO/graphene composites synthesized via HMTA-ZA route containing: (top) 2, (center) 5 and (bottom) 15 wt.% of graphene.

Effect of graphene addition - summary

As evident from the microstructural features of the ZnO rods in the composites, the presence and proportion of graphene seem to impart considerable influence on the morphological attributes of ZnO particles. As discussed above, the rods evolved from HMTA-ZA synthesis route were the shortest while the longest ones resulted with urea-ZN. The mode and pathway of ZA dissociation in aqueous solution and its subsequent interaction with the urea or HMTA is different from that of ZN. Consequently, the rate of nucleation and growth of ZnO nanoparticles from ZA is slower than from ZN. With ZA, more time is provided for the ZnO particles to form and grow resulting in a morphology that is most preferred in structure and shape with sharp and well-defined hexagonal edges. Also, when ZN is used as zinc source, the resulting rods are agglomerated as bundles; this is more evident in the case of HMTA than with urea. Incorporation of graphene seems to direct the formation of ZnO as uniform hexagonal rods, particularly when ZA is employed.

The effect of graphene on the aspects ratio of ZnO made from different precursors and reducing agents is summarized in Figures 21 and 22.

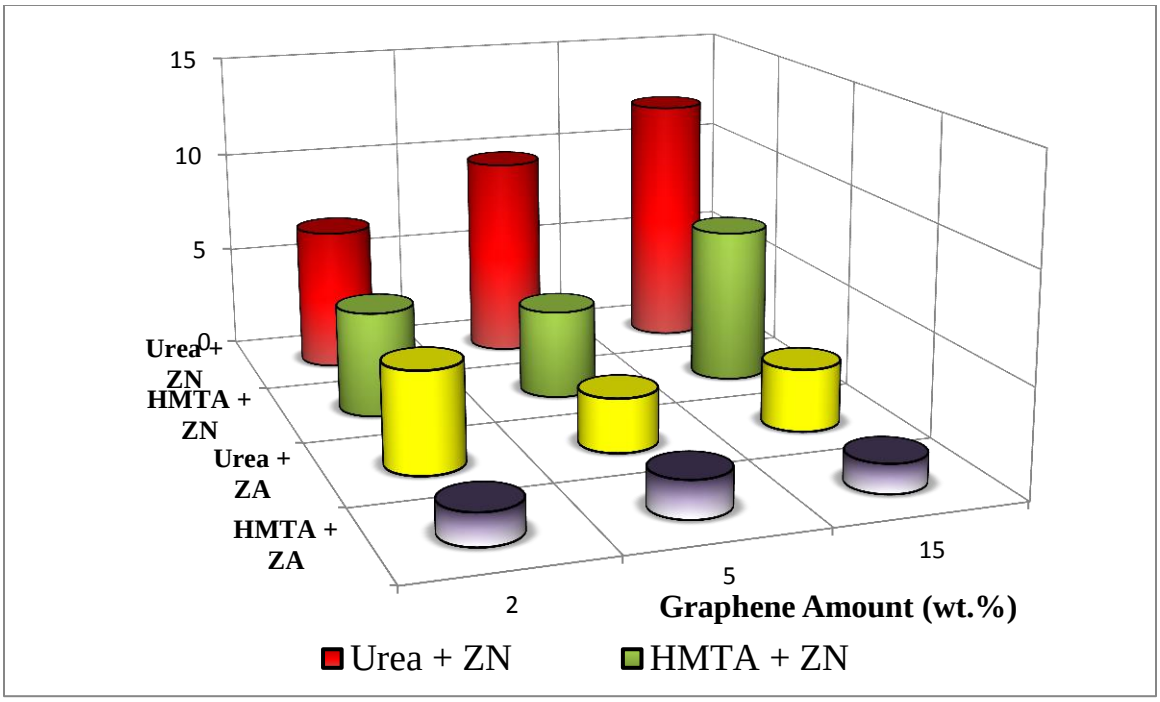

Figure 21: Dependency of aspect ratio of ZnO rods on graphene content.

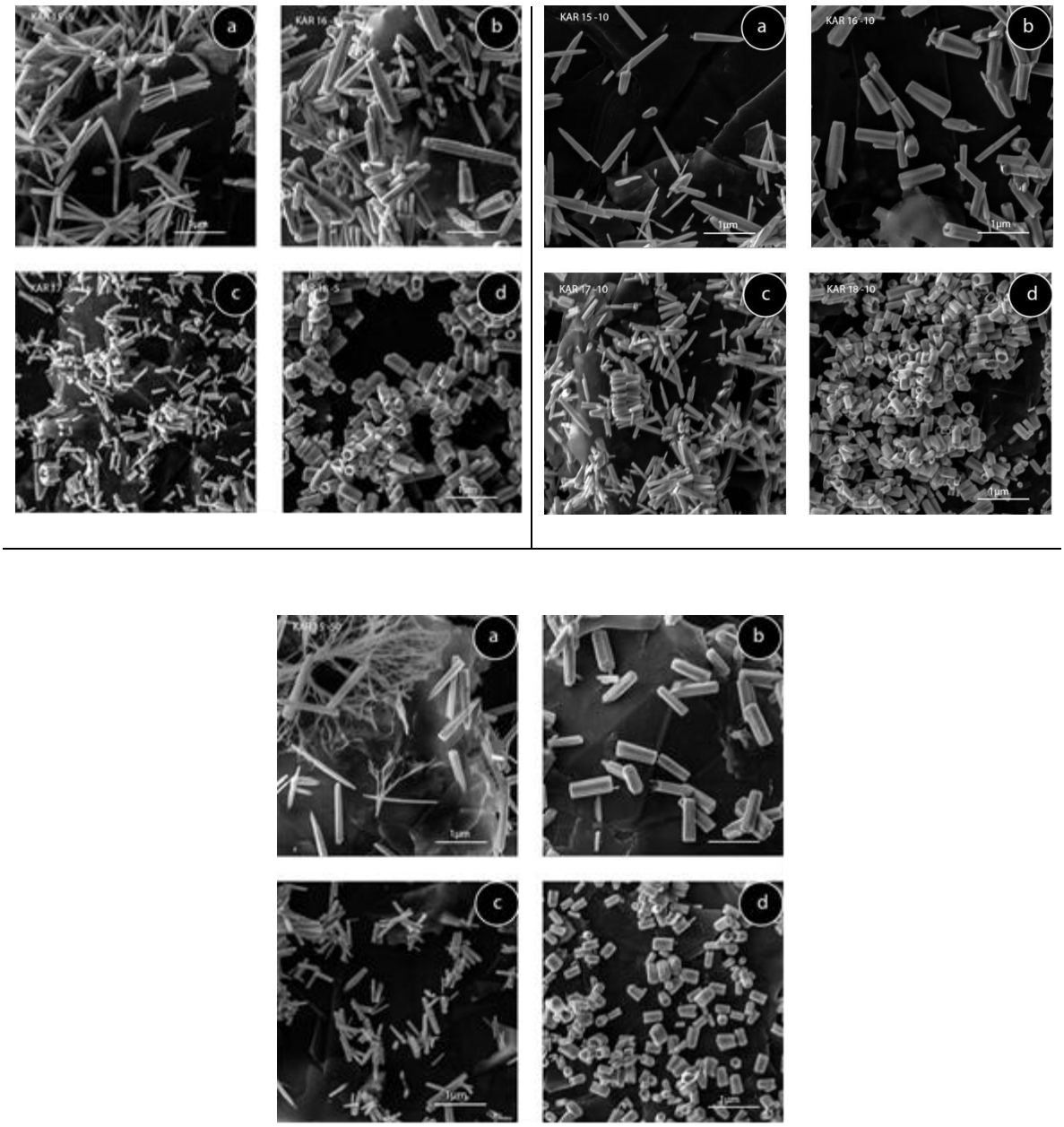

Figure 22: **Morphological variation in ZnO with: 2 (left), 5 (right) and 15 wt.% (bottom) graphene. a: urea-ZN, b: urea-ZA, c: HMTA-ZN and, d: HMTA-ZA.**

4.3. V_2O_5-ZnO/graphene composites

Several reports have suggested that the presence of vanadium oxide (V_2O_5) shows increase in the piezoelectric efficiency of ZnO [12, 43, 51, 52]. Thus, with the goal of studying the effect of vanadium incorporation on the morphological and piezoelectric behavior of ZnO composite, several formulations of V_2O_5-ZnO were synthesized by modifying the earlier recipe suitably. Vanadium was introduced in solution in the form of ammonium metavanadate (NH_4VO_3).

4.3.1. Calculation

It was decided to incorporate 2.5, 5 and 10 wt.% of V_2O_5 using ammonium metavanadate (NH_4VO_3) precursor. For this, the amount of NH_4VO_3 to yield V_2O_5-ZnO composite, was calculated as follows:

FW of $Zn(NO_3)_2.6H_2O$ = 297.4815 Dalton

FW of $Zn(COOCH_3)_2.2H_2O$ =219.51 Dalton

FW of NH_4VO_3 = 116.98 Dalton

FW of V_2O_5 = 181.88 Dalton

Solubility of NH_4NO_3 in water: 4.8 g/L at 20°C

The dissolution of ammonium metavanadate in water and formation of upon decomposition during reflux in aqueous urea or HMTA solution could be represented as:

$$NH_4VO_3 + H_2O \rightarrow NH_4OH + HVO_3 \quad (10)$$

$$2HVO_3 \rightarrow V_2O_5 + H_2O \quad (11)$$

$$2NH_4VO_3 + H_2O \rightarrow V_2O_5 + 2NH_4OH \quad (12)$$

Therefore, according to Eq. (12),

$$2\ moles\ NH_4VO_3 \equiv 1\ mole\ of\ V_2O_5 \quad (13)$$

By definition,

$$116.89\ g\ of NH_4VO_3\ in\ 1000\ ml\ of\ water \equiv 1\ M$$

Based on solubility data,

$$\rightarrow 4.8\ g\ of NH_4VO_3\ in\ 1000\ ml\ of\ water \equiv 0.041\ M$$

$$\therefore 0.041\ M\ NH_4VO_3\ in\ 100\ ml\ of\ water \equiv 0.48\ g\ of\ NH_4VO_3\ in\ 100\ ml\ of\ water$$

$$\therefore 1\ ml\ of\ 0.041\ M\ NH_4VO_3\ solution\ contains\ 0.0048\ g\ NH_4VO_3 \quad (14)$$

To calculate the amount of NH_4VO_3 to yield 2.5, 5 and 10 wt.% of V_2O_5 in ZnO, first the theoretical yield of ZnO from ZN and ZA was calculated as follow:

ZnO from $Zn(NO_3)_2.6H_2O$:

297.4815 g of $Zn(NO_3)_2.6H_2O$ yields 81.408 g/mole of ZnO.

Based on the preparation conditions, ZN solution contains 10.4119 g $Zn(NO_3)_2.6H_2O$ in 100 ml of water. Therefore, the amount of ZnO obtained from this solution is:

$$x = \frac{81.408 \times 10.4119}{297.4815} = 2.85 \text{ g of ZnO in 100 ml of water}$$

Since in a typical batch synthesis, 10 ml of $Zn(NO_3)_2.6H_2O$ was added to the refluxing solution, the theoretical amount of ZnO from each batch = 0.285 g.

ZnO from $Zn(COOCH_3)_2.2H_2O$:

219.51 g of $Zn(COOCH_3)_2.2H_2O$ yields 81.408 g/mole of ZnO.

The zinc precursor from ZA contains 7.6829 g $Zn(COOCH_3)_2.2H_2O$ in 100 ml of water. Therefore, the amount of ZnO obtained from this solution is given by

$$x = \frac{81.408 \times 7.6829}{219.51} = 2.85 \text{ g of ZnO in 100 ml of water}$$

Since in a typical batch synthesis, 10 ml of $Zn(COOCH_3)_2.2H_2O$ is added to the refluxing solution, the theoretical amount of ZnO from each batch = 0.285 g.

Therefore the theoretical yield of ZnO from ZN and ZA = 0.285 g

Thus, 2.5 wt.% of ZnO = 0.007125 g

Similarly, 5 wt.% of ZnO = 0.01425 g

And, 10 wt.% of ZnO = 0.0285 g

From eq. (13):

$$2 * 116.98\ g\ of\ NH_4VO_3 \equiv 181.88\ g\ of\ V_2O_5$$

So, 2.5 wt.% V_2O_5 (0.007125 g) can be obtained from:

$$\frac{2 \times 116.98}{181.88} \times 0.007125 = 0.0093\ g\ of\ NH_4VO_3$$

5 wt.% V_2O_5 (0.01425 g) can be obtained from:

$$\frac{2 \times 116.98}{181.88} \times 0.01425 = 0.01833\ g\ of\ NH_4VO_3$$

10 wt.% V_2O_5 (0.0285 g) can be obtained from:

$$\frac{2 \times 116.98}{181.88} \times 0.0285 = 0.03666\ g\ of\ NH_4VO_3$$

Finally, From Eq. (14):

$$1\ ml\ of\ \ 0.041\ M\ NH_4VO_3\ contains\ 0.0048\ g\ NH_4VO_3$$

$\therefore$ 0.007125 g of V_2O_5 is obatined $from$ 1.93 $ml\ of$ 0.041M NH_4VO_3 (2.5 % V_2O_5)

Similarly,

0.01425 g of V_2O_5 is obatined $from$ 3.82 $ml\ of$ 0.041M NH_4VO_3 (5 % V_2O_5)

And, 0.0285 g of V_2O_5 is obatined $from$ 7.64 $ml\ of$ 0.041M NH_4VO_3 (10 % V_2O_5)

4.3.2. V_2O_5-ZnO/graphene composites using urea and ZN/ZA

V_2O_5-ZnO/graphene particles containing different levels of V_2O_5 loading were prepared from ZN or ZA and 0.041 M NH_4VO_3 solution in the presence of 2 wt.% graphene by refluxing with aqueous urea or HMTA, as per the methodology developed and described in section 3.2.5. The phase identification was carried out by performing powder X-ray diffraction and the presence of vanadium has been confirmed by EDS. The SEM images of the V_2O_5-ZnO/graphene sample using urea-ZN route are shown in Figure 23, where the effect of V_2O_5 addition (using aqueous NH_4VO_3 solution) on the morphology of ZnO particles is quite evident. For example, in the case of 2.5 wt.% V_2O_5-ZnO/graphene samples (Fig. 23 A-B), the particle size distribution was rather large with significant degree of agglomeration. In addition, the typical familiar hexagonal rod structure was replaced by long pencil-shaped structure terminating in pointed ends. The degree of agglomeration increased further with V_2O_5 content (5 wt.% V_2O_5/ Fig.23 C) with flower-like microstructure accumulating on the tip of the rods. When the amount of V_2O_5 was increased to 10 wt.%, a mixture of 3-D hexagonal pencil-shaped rods and 2-D hexagonal platelets were obtained (Fig. 23 D).

In the case of urea-ZA, however, the typical hexagonal rod-like motif is almost completely destroyed and replaced by agglomerations of porous 2-D platelets and flower petal-like morphology, as shown in Figure 24, in the presence of 10 wt.% V_2O_5.

From this, it appears that the presence of V_2O_5 disrupts systematic morphological evolution in the case of urea-derived ZnO.

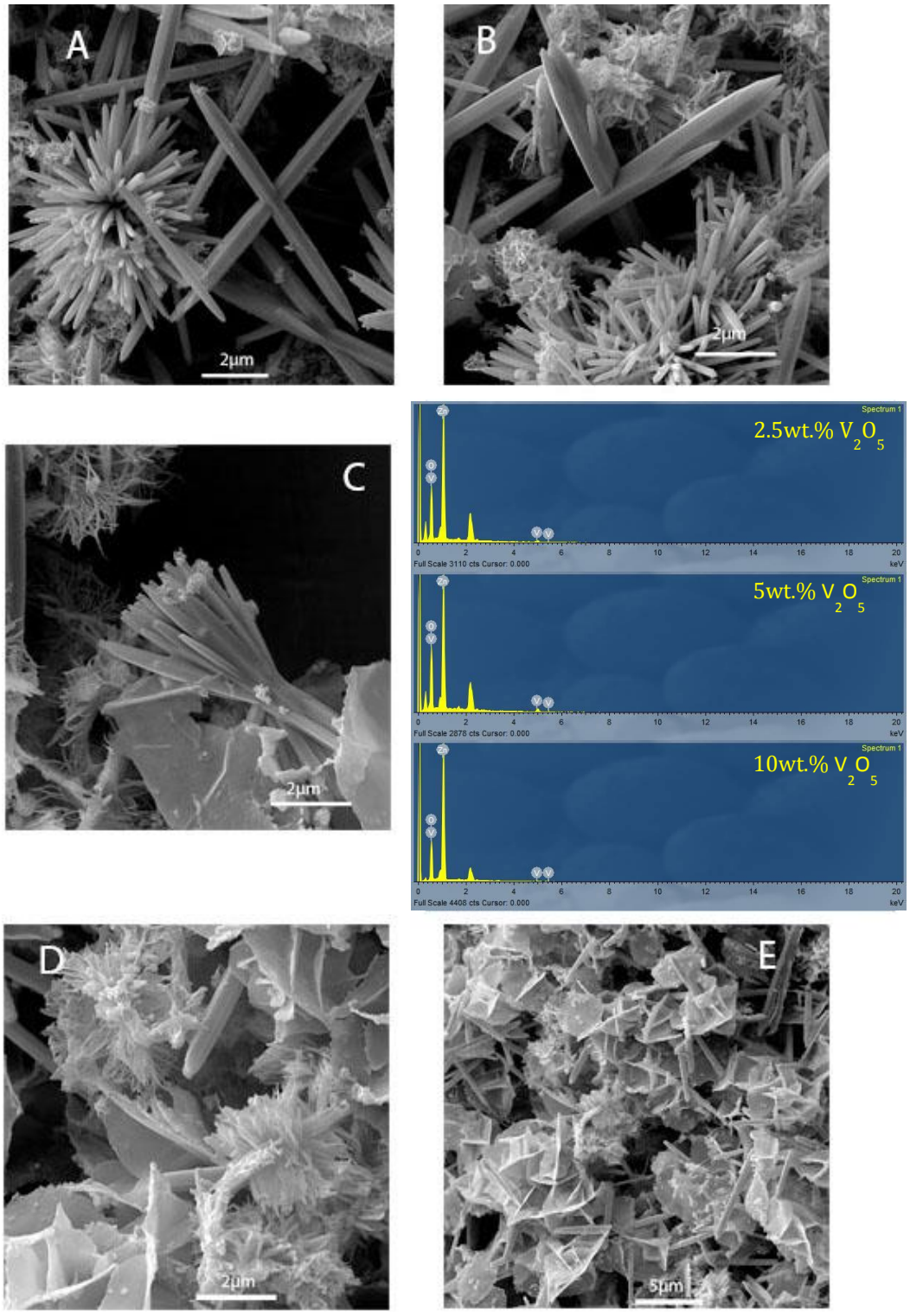

Figure 23: SEM images of V_2O_5-ZnO/graphene composites synthesized from urea-ZN with: 2.5 (A-B), 5 (C) and 10 wt.% V_2O_5 (D-E). The EDS signatures are also shown.

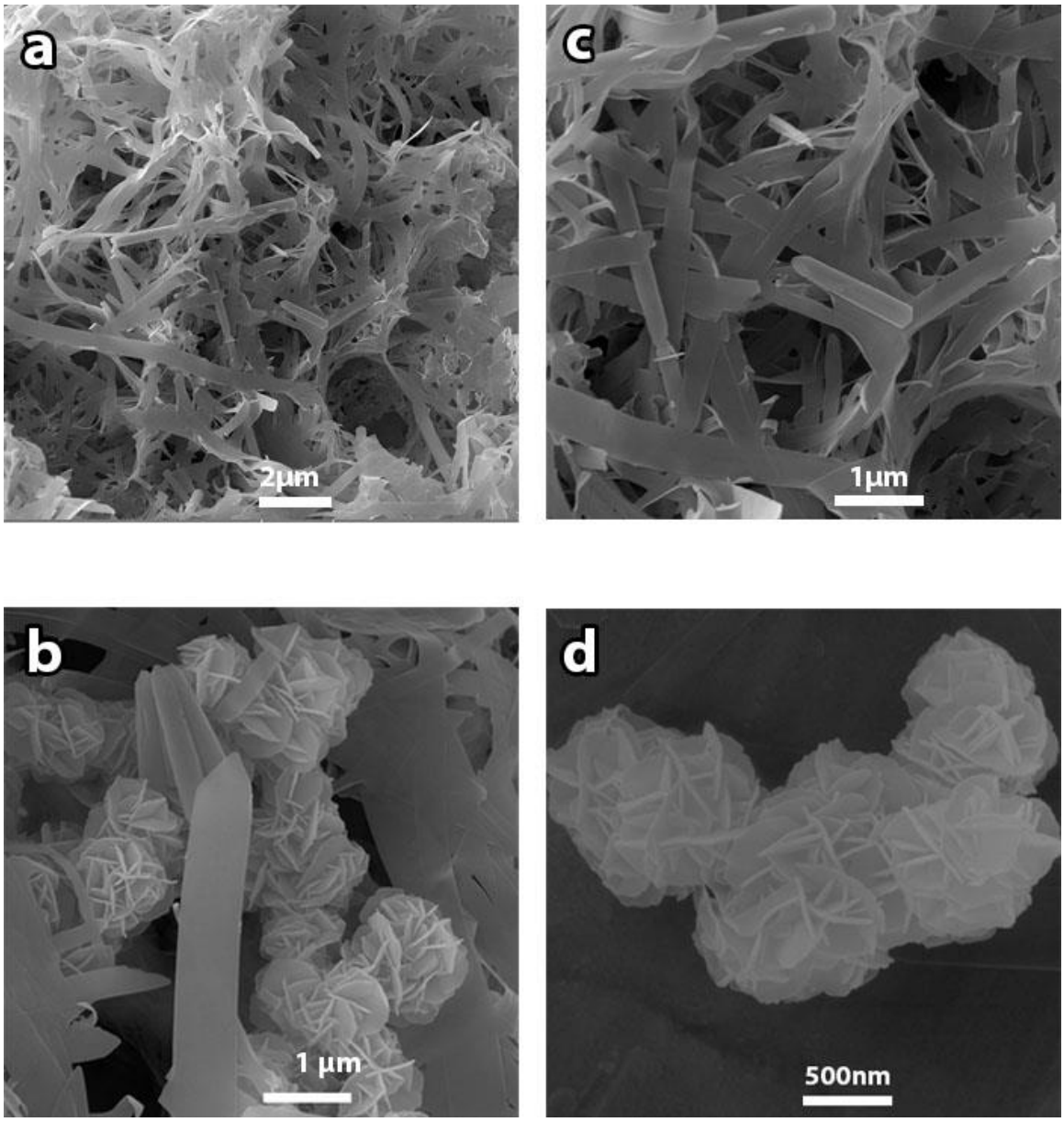

Figure 24: SEM images of V_2O_5-ZnO/graphene composite synthesized from urea-ZA with 10 wt.% V_2O_5.

4.3.3. V_2O_5-ZnO/graphene composites using HMTA and ZN/ZA

a. Structural characterization

The XRD patterns of V_2O_5-ZnO/graphene made via HMTA-ZN or HMTA-ZA route are shown in Figure 2.As was the case with pure and graphene augmented ZnO samples, the diffraction patterns accounted for ZnO and graphene alone. In addition, peaks due to trizinc dihydroxide divanadate dihydrate [$Zn_3(OH)_2(V_2O_7)$ $(H_2O)_2$] and Shcherbinaite (V_2O_5) in traces were also detected. Indepenedent TGA and DSC analysis showed that NH_4VO_3 decomposes into V_2O_5 below 400°C temperature. Based on that, the as-made V_2O_5-ZnO/Gr samples were heated up to 400°C in static air and XRD examination was performed on the product; the diffraction patterns are shoown in Figure 26. As can be seen, all the diffraction peaks now correspond to ZnO, graphene, and V_2O_5 (traces) alone and no other impurities could be detected.

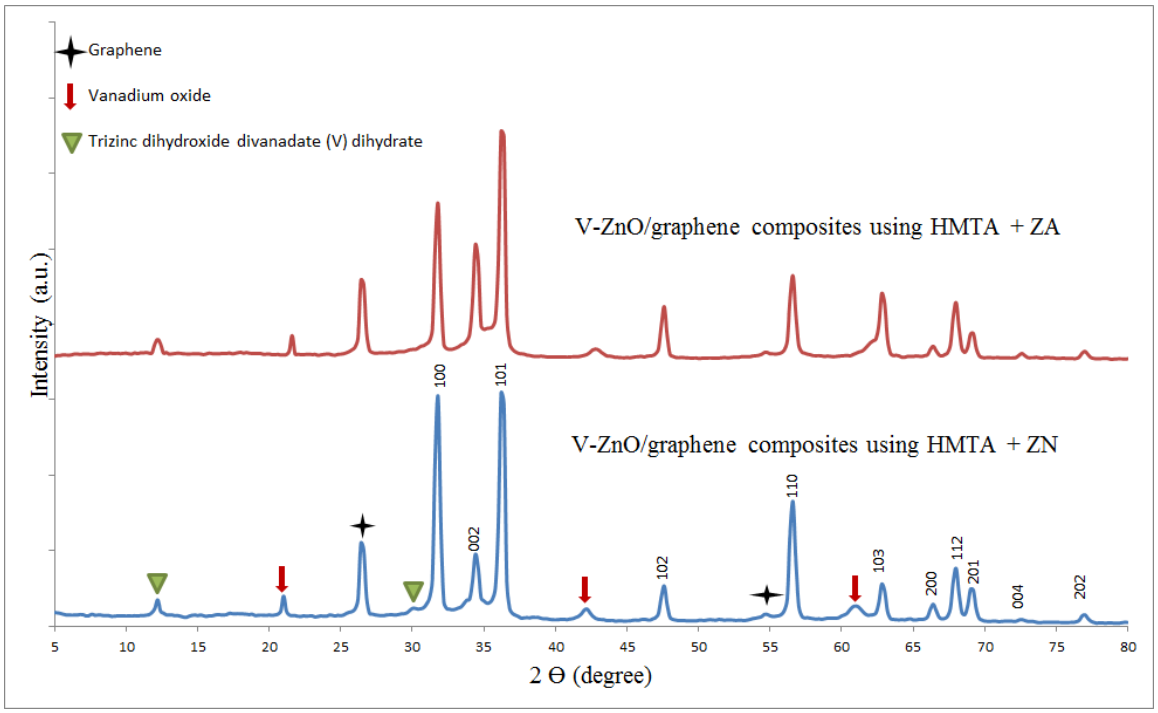

Figure 25 XRD patterns of as-synthesized 5% V_2O_5-ZnO/graphene composite from HMTA-ZA and HMTA-ZN routes

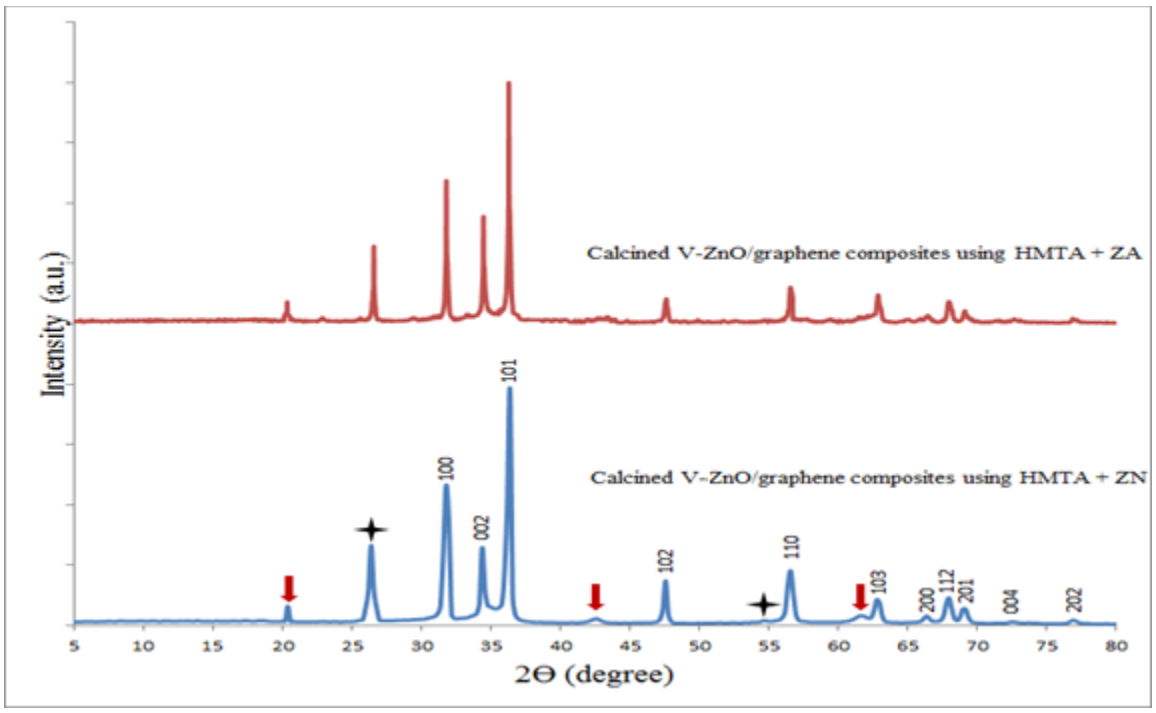

Figure 26: XRD patterns of the 5% V_2O_5-ZnO/graphene composite powder calcined at 400°C/1 h

b. Microstructural characterization

Systematic variations in the weight fraction of V_2O_5 appears to control the ultimate shape and size of ZnO in the modified samples compared to the predominantly rod morphology observed with pure or graphene added ZnO or synthesized under identical conditions. The prominent effect of three levels of V_2O_5 additive on the morphology of HMTA-ZN and HMTA-ZA-derived ZnO is illustrated in Figures 27, 28, and 29. These images show that precise tailoring of microstructure at nanoscale (from 3-D nanorods to flower-petal aggregates to 2D nanoplatelets) is achievable by simple tweaking of the ratio of zinc to vanadium in the reaction mixture. The TEM images of 5 wt. % V_2O_5-ZnO/Gr composites synthesized by HMTA-ZN route shown in Fig.30 are evidence of the hexagonal platelets as well as the transparency of the rods (due to the formation of ZnO tubes). The TEM images of 10 wt. % V_2O_5-ZnO/Gr composites synthesized by HMTA-ZN route are shown in Fig.31, which clearly shows significant reduction is particle size.

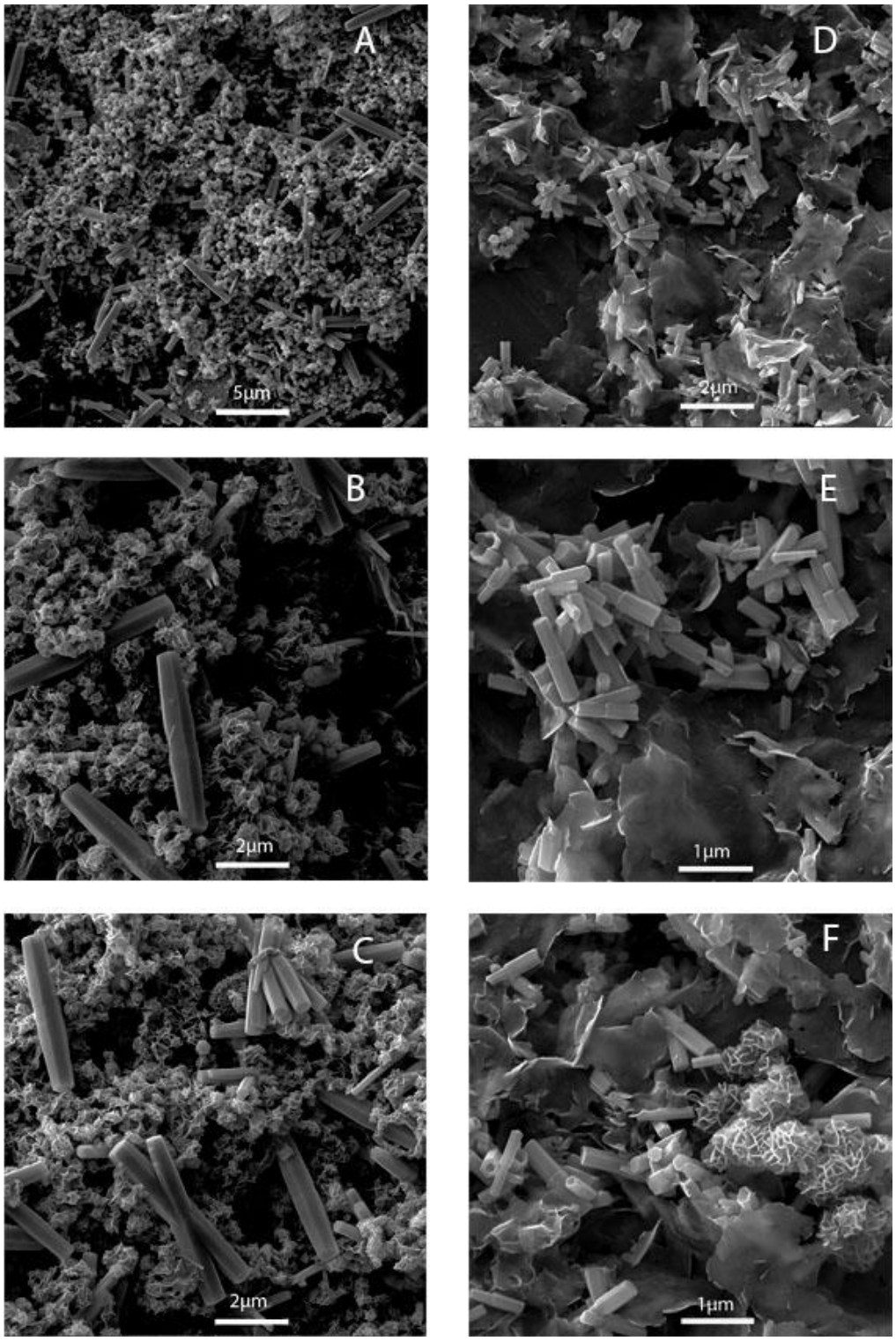

Figure 27: SEM images of 2.5 wt. % V_2O_5-ZnO/graphene composites synthesized with HMTA and: (left) ZN and (right) ZA

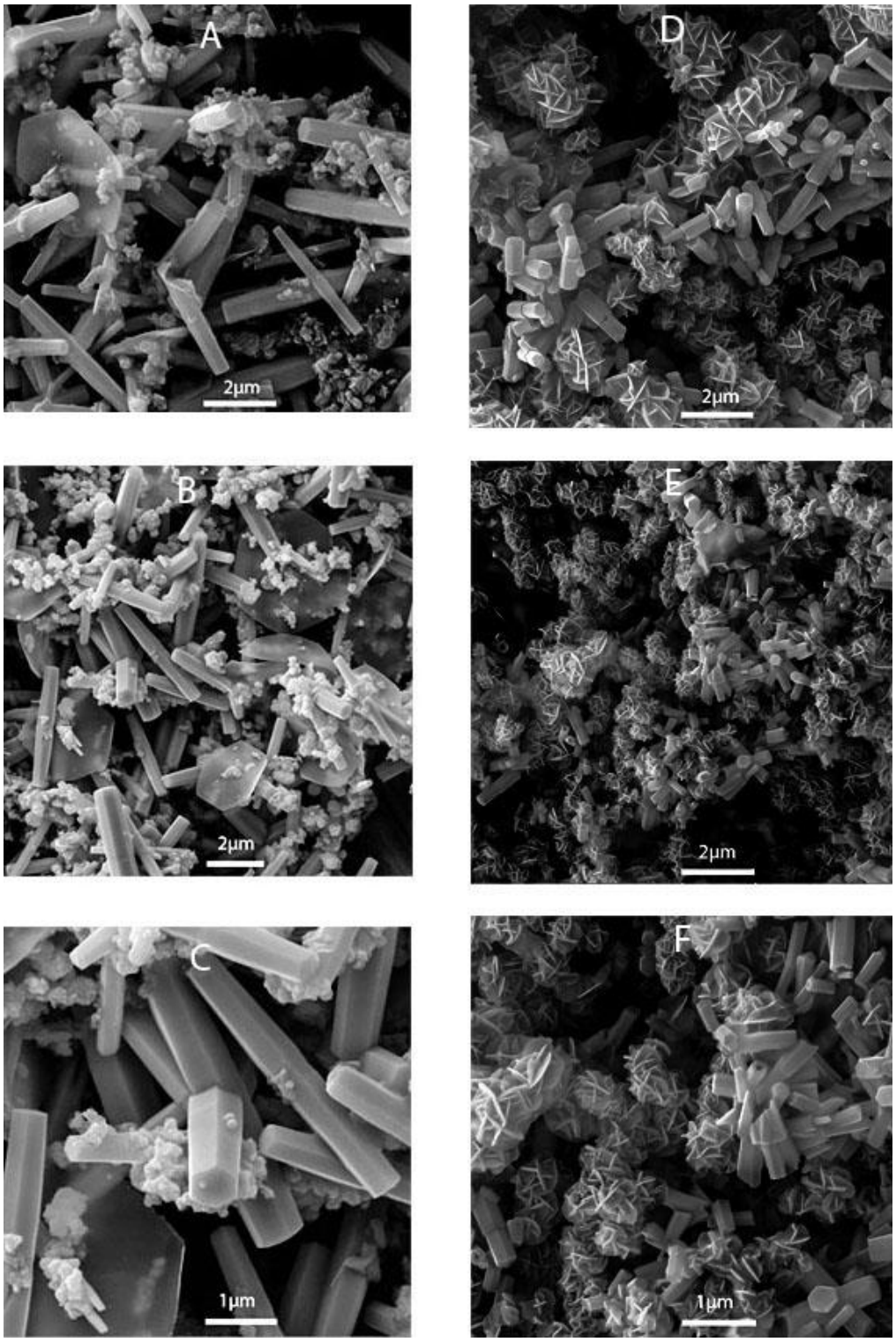

Figure 28: SEM images of 5 wt. % V_2O_5-ZnO/graphene composites synthesized with HMTA and: (left) ZN and (right) ZA

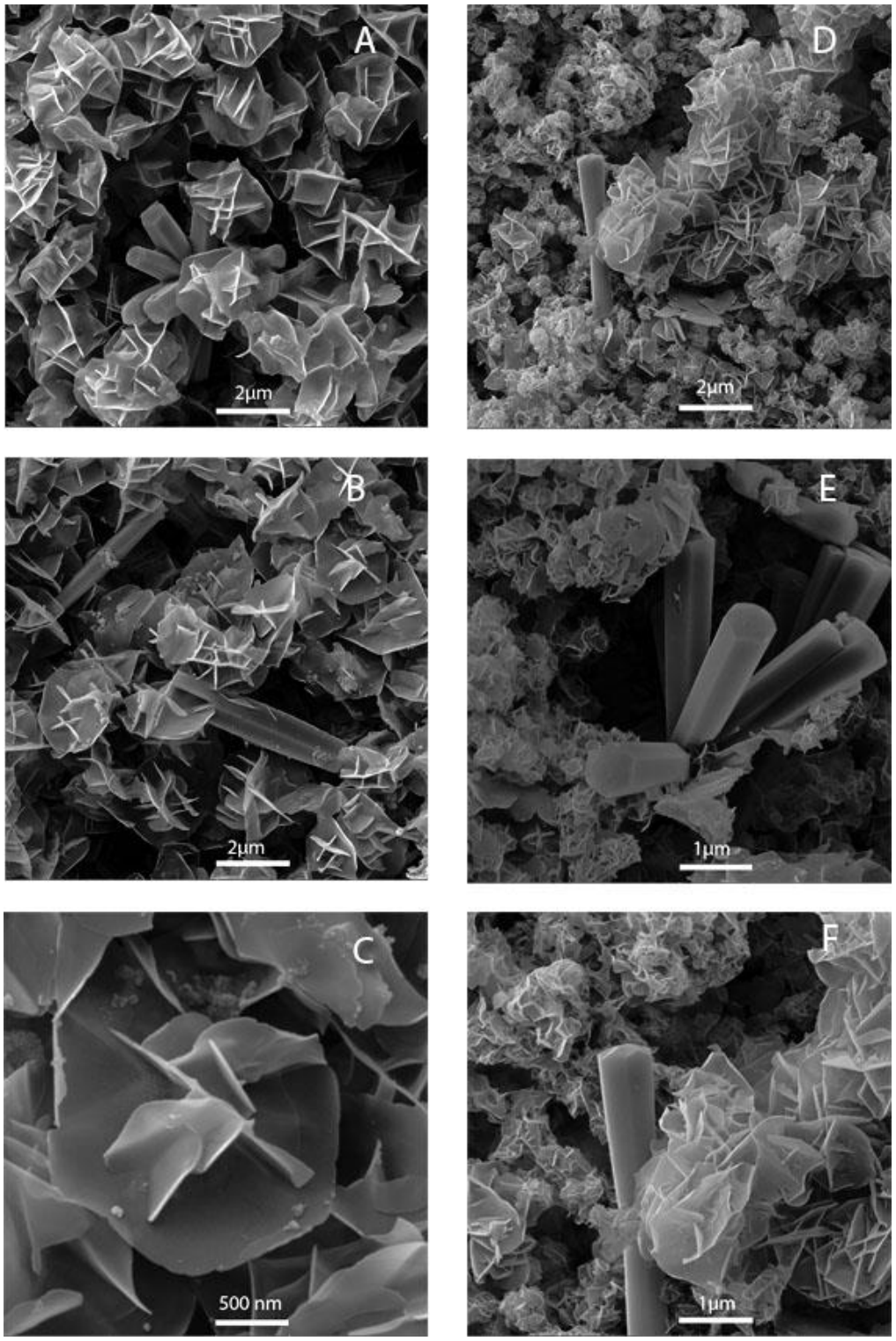

Figure 29: SEM images of 10 wt. % V_2O_5-ZnO/graphene composites synthesized with HMTA and: (left) ZN and (right) ZA

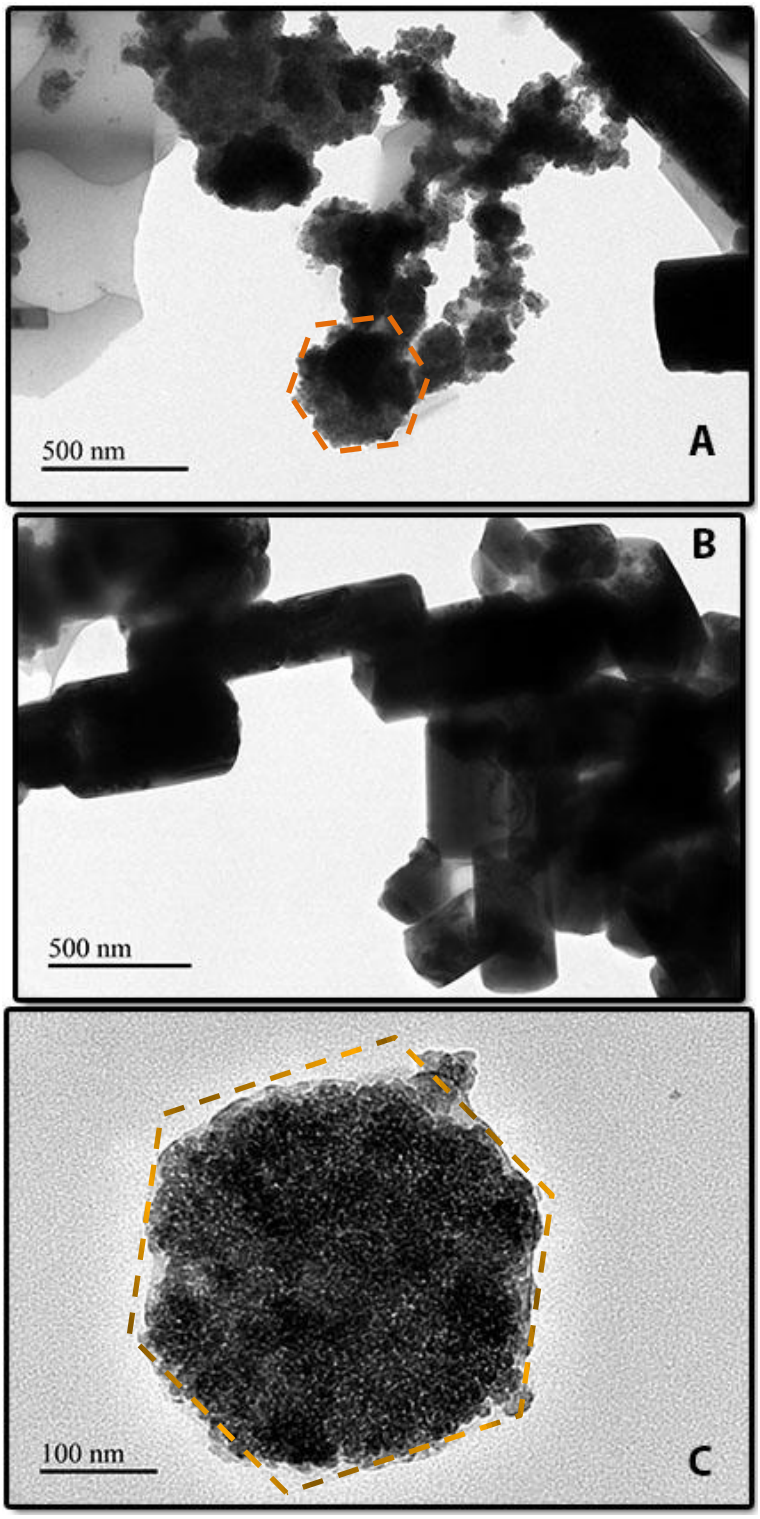

Figure 30: TEM images of 5 wt. % V_2O_5-ZnO/graphene composite synthesized by HMTA-ZN route.

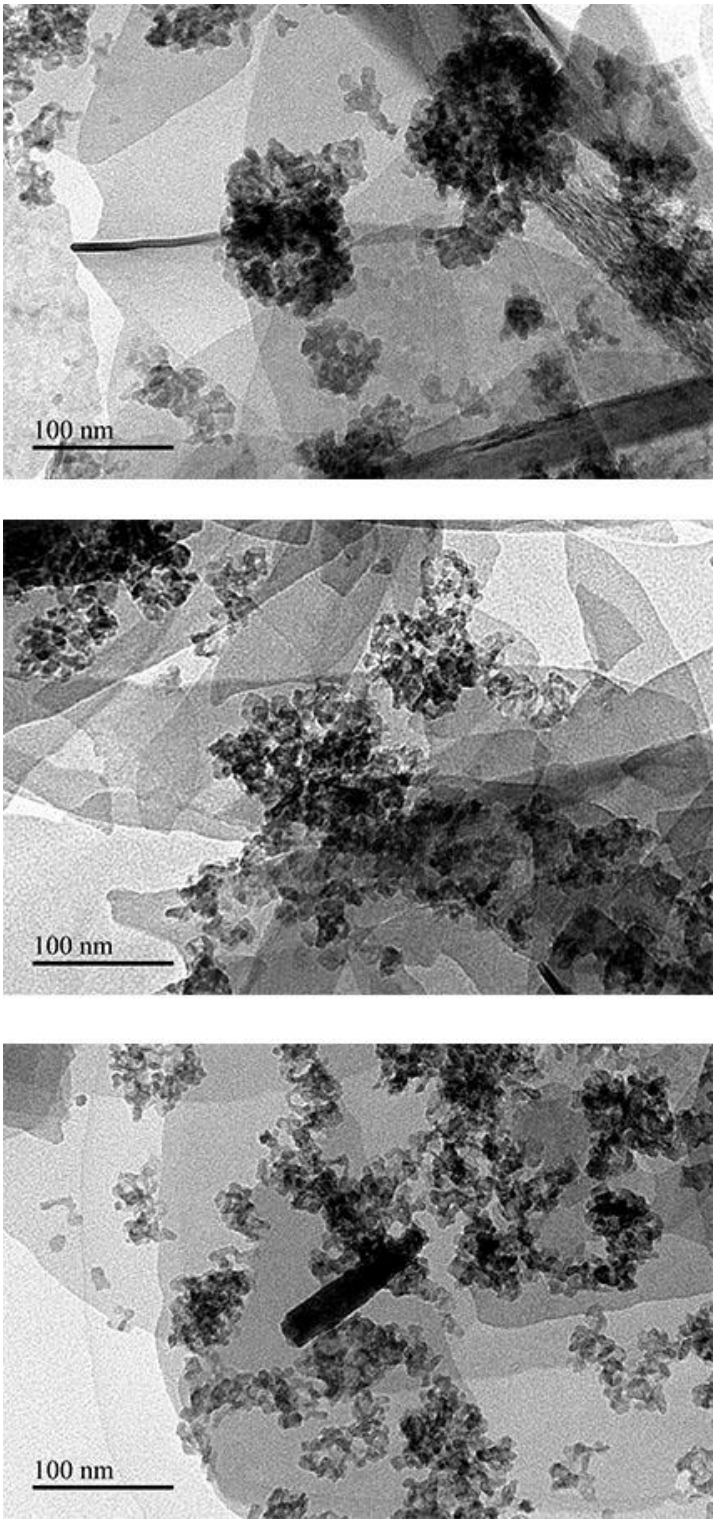

Figure 31: TEM images of 10 wt.% V_2O_5-ZnO/graphene composites synthesized by HMTA-ZN route.

4.4. Fabrication of ZnO-based energy harvesting device

The ZnO-based energy harvesting device (EHD) was fabricated by blending various amounts of pure ZnO/graphene in one case and 5 wt.% V_2O_5-ZnO/graphene composites with 10 wt.% polyvinylidene difluoride (PVDF) solution. Initially, PVDF powder was dissolved separately in two solvents: N,N-dimethylacetamide (DMAc) and acetone. PVDF could be dissolved in DMAc at room temperature under constant stirring for several hours. PVDF dissolved completely in acetone around 55°C within a short time. As prepared, both solutions are clear and stable. However, it was found that the solution in acetone was easy to work with, in addition to its obvious advantage being environmentally friendly and less toxic than DMAc. The films were cast at room temperature and atmospheric pressure in a vibration-free location of the laboratory; The PVDF-acetone solution could be cast into film within 2 h, whereas it takes 16-20 h in the case of DMAc; any vibration or disturbance in the vicinity of the cast would cause formation of wrinkles/ripples throughout the cured film, which is undesirable. As can be seen from Figure 32, the PVDF film from acetone solution is translucent, while that from DMAc is opaque.

The difference could be attributed to the method of solution preparation, the dissolution temperature and its effect on the polymeric chains present in PVDF. For example, even though, both DMAc and acetone are polar solvents, heating up to ~55°C in the second case, assists in somewhat unwinding and untwining the steric bonds in PVDF, which is not likely in the case of room temperature dissolution process when DMAc was used. This gives rise to the difference in the light absorption and transmittance in the two cases. The choice of solvent also affected the nature of dispersion of ZnO/graphene composite

particles. Thus, as can be seen from Figure 33, the cast film was homogeneous and uniform on both sides when acetone was used, whereas in the case of films made in DMAc, the top of the film was dark gray while the opposite side was white.

Based on these iterations and the relative ease of casting ceramic-polymer composites as homogeneous films, EHD devices were fabricated using 10 wt.% PVDF solution in acetone. The loading of ZnO/Gr and V_2O_5-ZnO/Gr in the composite was systematically varied from 10, and 20 wt.% to 40 wt.%. Thus, for making the cast in a typical case, 0.1, 0.2 and 0.4 g of the ceramic/Gr composite powder was mixed with 10 ml of PVDF-acetone solution, thoroughly homogenized by vigorous magnetic stirring and poured into a polycarbonate ring (3-in. diameter and ½-in. wall height), secured firmly on a dense 6 in. x 6 in. alumina plate. In each of these formulations, loading of graphene was kept constant at 2 wt.% (with respect to amount of ZnO). Similarly, in the case of V_2O_5-ZnO/Gr, the amount of V_2O_5 was kept constant at 5 wt.% (relative to amount of ZnO).

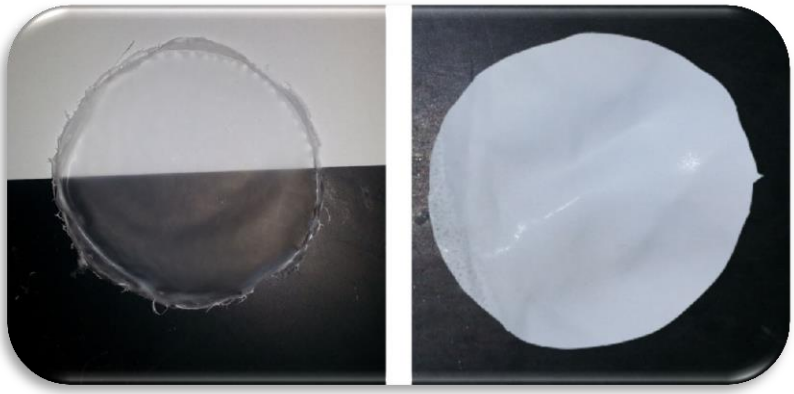

Figure 32: PVDF film cast from acetone (left) and DMAc (right)

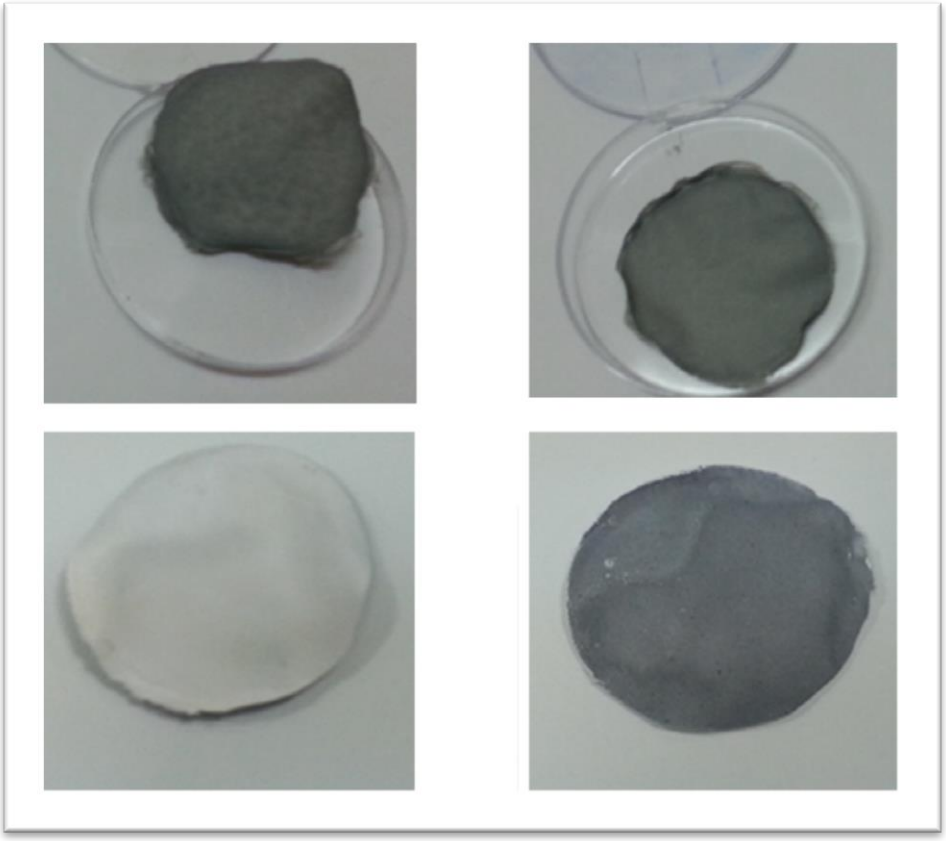

Figure 33: Photographs of top and bottom layers of the ZnO/Gr films cast with PVDF solution in acetone (top) and DMAc (bottom)

4.4.1. Poling of ceramic-polymer films

The ceramic-polymer composite casts were poled to align the piezoelectric domains in ZnO as well as in PVDF by applying high voltage across it. Upon poling, PVDF shows efficient piezoelectric behavior. Prior to poling, the cast films were coated with thin layer of a room temperature conductive paste (Anders Products, US) on both sides. After drying the paste, the specimen was placed between two thin rectangular (3 in. x 2 in. x 0.04 in) stainless steel plates, each attached with electrical wires as shown in Figure 34. The electrical set-up used in this work is shown in Fig.35. A high voltage source (Canberra, model 3002) was connected to a digital multimeter DMM (Fluke, model 87) in series through a pair of known resistances and the sample completing the circuit. The DMM across the sample was used to monitor leakage current during poling. From safety consideration, a 10 MΩ resistor was connected in series to the HV source. In addition, two more resistors (4 MΩ and 400 MΩ) in series were placed in parallel to the sample and voltage across the 4 MΩ resistor was measured. Each film was poled by applying ~200V/cm across it.

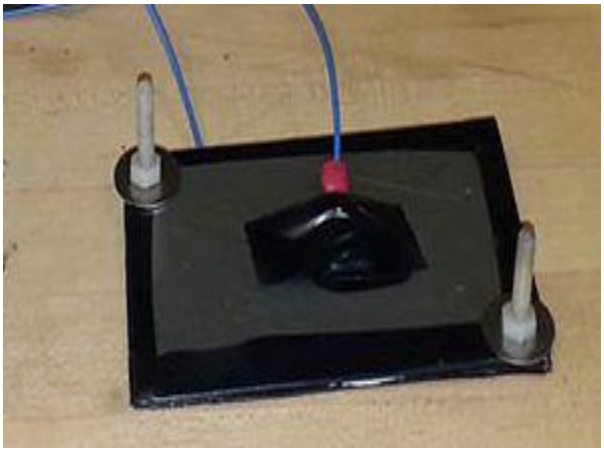

Figure 34: Sample preparation for poling

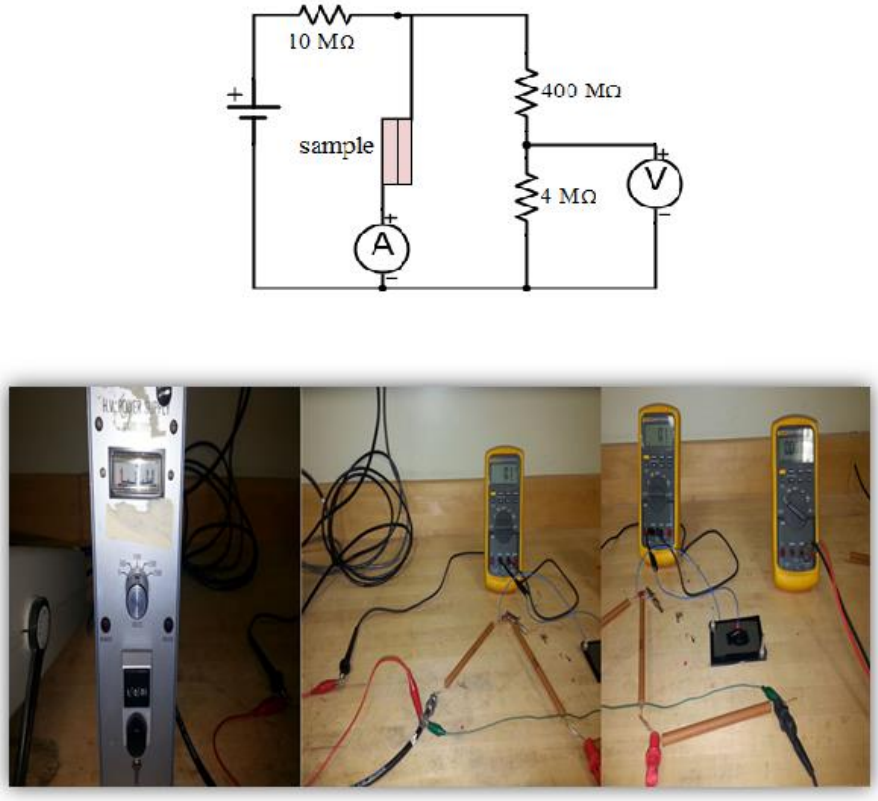

Figure 35: Circuit diagram (top) and image of the actual set-up (bottom) used for poling

4.5. Energy harvesting experiments

The mechanical deformation-electrical voltage stimulus of various formulations developed in this research was collected by bending and unbending the devices manually and measuring the open circuit voltage using GW Instek GDS-2021 Digital Oscilloscope (Taiwan). The oscilloscope is shown in Figure 36. Measurements were repeated on a given samples, five or more number of times to verify the consistency, repeatability and reproducibility of the data obtained. The electrical output was measured during periodic bending and unbending action. The direction of the signal (voltage spike) shown in Figures 37 and 38 is corresponded to bending and unbending of the cast films of difference formulations. Upon bending, an impact pressure/force is applied on the specimen, generating a piezoelectric potential due to the compressive strain, which makes electrical charges flow from low-potential end to the high-potential, that get accumulated in the material to balance the piezoelectric potential. When the stress is released, the accumulated charges flow in the opposite direction. For this reason, in each period, positive and negative voltage signals were observed. Since the deformation imposed was manual in nature, it is natural that the stress applied in each case was not identical, leading to somewhat different stimulus in every subsequent run. For the same reason, it is very likely that the maximum value generated by the device were not captured sometime. Therefore, among the recorded data for each sample, the one registering highest values was used in generating the plots.

Figure 36: Digital oscilloscope used in the electrical measurement

4.5.1. Performance of (ZnO/Gr)-PVDF composite

1. ZnO from Urea - (ZN/ZA)

The electrical output of ZnO/Gr/PVDF composite with ZnO obtained from urea-ZN or urea/ZA route is summarized in Figure 37 for 10, 20 and 40 wt.% loading of the ZnO-Gr composite. As can be seen, the response of the composite containing ZN-derived ZnO was higher than that from ZA. The increase in the voltage was commensurate with increasing amount of ZnO in both cases. However, the highest response was registered with composite containing 20% ZnO (21.5 V) in the case of ZN and 40% ZnO (25.5 V) from ZA.

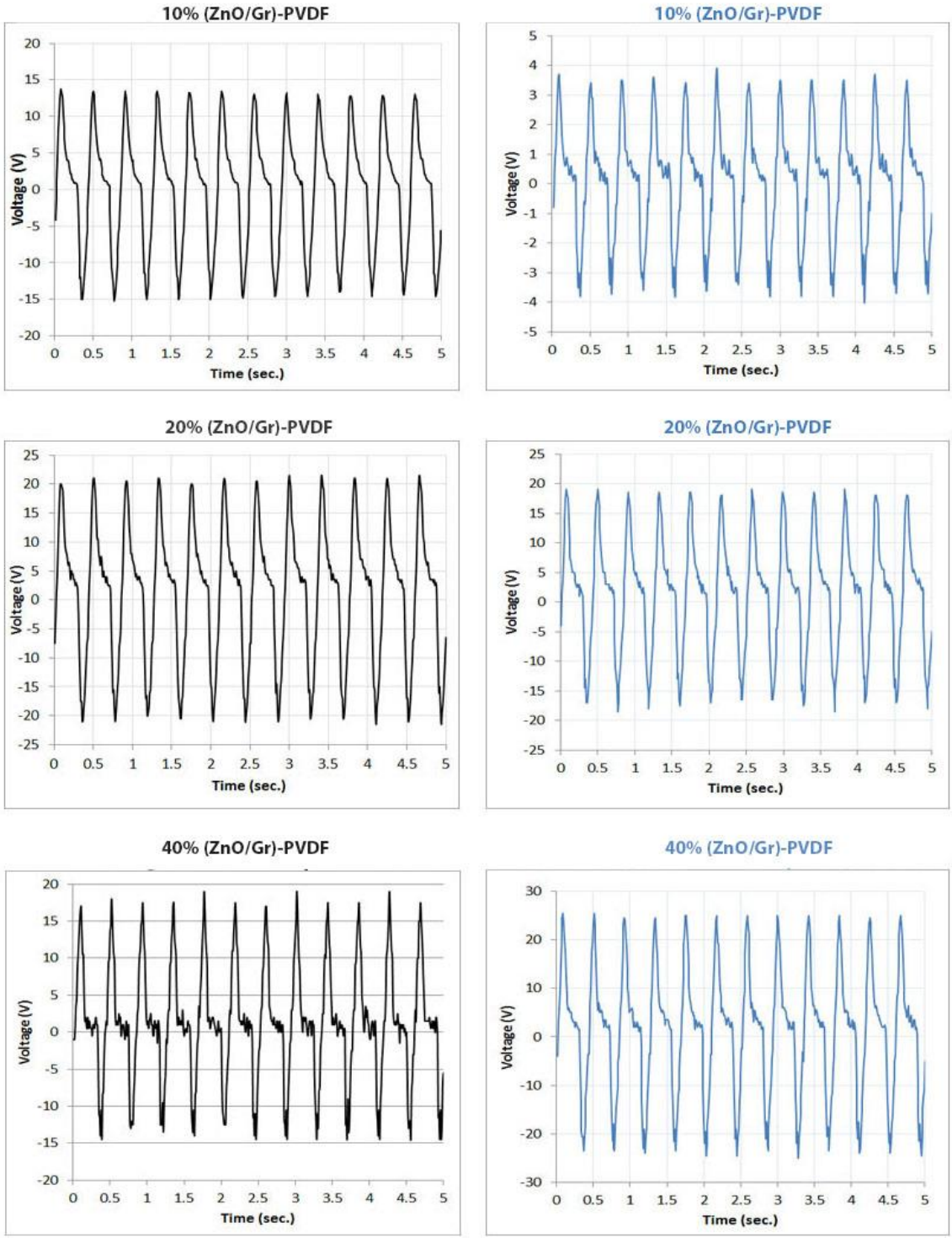

Figure 37: Open circuit voltage response to bending and unbending of ceramic-polymer composites containing 10, 20 and 40 wt.% ZnO/Gr from urea-ZN (L) and urea-ZA (R)

2. ZnO from HMTA - (ZN/ZA)

The electrical output of ZnO/Gr/PVDF composite with ZnO obtained from HMTA-ZN or HMTA/ZA route is shown in Figure 38 for 10, 20 and 40 wt.% loading of ZnO/graphene. In this case also, the response of the composite containing ZnO derived from ZN was higher than that using ZA. Increase in the output voltage was systematic and monotonic with increase in the amount of ZnO. However, the highest response was registered with 20% ZnO (23 V) from ZN and with 40% ZnO (11 V) from ZA in the composite. The lowering of electrical stimuli is composites containing higher (> 20%) ZnO/graphene together with V_2O_5 could be attributed to the stiffness (lack of flexibility) of the resulting formulation and significant change in microstructure (replacement of ordered 3-D hexagonal rods with random flower-petal-like 2-D sheets); increasing amount of ceramic in the composite led to higher rigidity and limited flexibility to deformation.

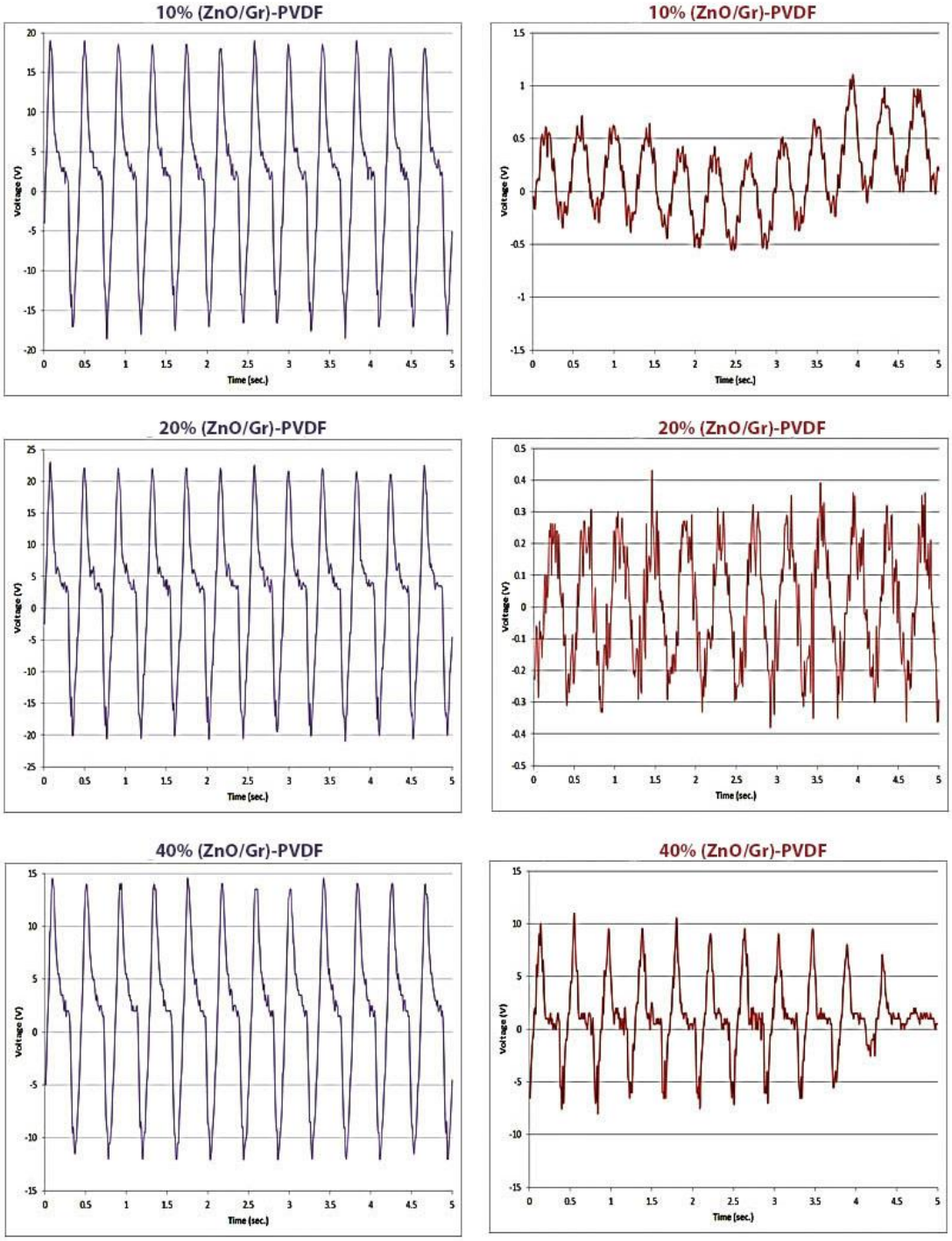

Figure 38: Open circuit voltage response to bending and unbending of ceramic-polymer composites containing 10, 20 and 40 wt.% ZnO/Gr from HMTA-ZN (L) and HMTA-ZA (R)

3. 5 wt.% V_2O_5-ZnO/Gr-PVDF composite with ZnO from HMTA - (ZN/ZA)

As can be readily seen from data presented in Figure 39, the open circuit voltage output was consistently higher in the case of ZnO derived from HMTA-ZA; maximum signal was seen in samples containing 20 wt. % ZnO in the composite. The lowering of electrical stimuli is composites containing higher (> 20%) ZnO/graphene content could again be attributed to the stiffness (lack of flexibility) of the resulting formulation and significant change in microstructure (replacement of ordered 3-D hexagonal rods with random flower-petal-like 2-D sheets); increasing amount of ceramic in the composite led to higher rigidity and limited flexibility to deformation.

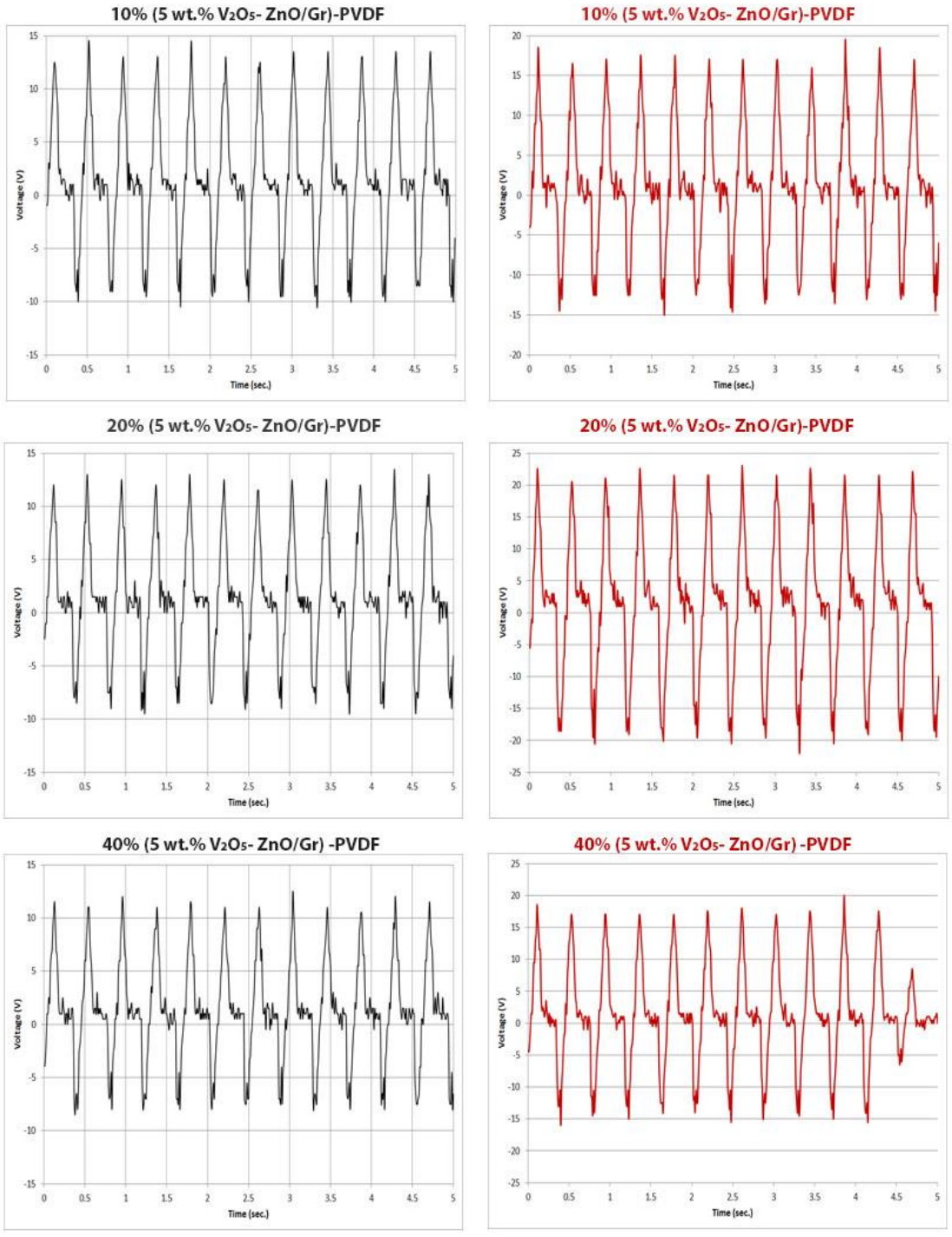

Figure 39: Open circuit voltage response to bending and unbending of composites containing 10, 20 and 40 wt.% of (5 wt.% V_2O_5- ZnO/Gr) from HMTA-ZN (L) and HMTA-ZA (R) in PVDF.

These results showing the effect of choice of source of zinc (ZN or ZA), choice of reducing agent (urea or TMHA) and V_2O_5 are compiled in Figure 40. As can be readily seen, highest output was generated by 40% (ZnO/Gr)-PVDF sample, where ZnO is derived from urea-ZA recipe while the minimum response was exhibited by 20% (ZnO/Gr)-PVDF specimen, where ZnO was derived from HMTA - ZA. This strongly suggests the effect of sharpness of the well-shaped rods with high crystallinity on the efficiency of EHD. Although the addition of V_2O_5 did not show the expected enhancement in the yield, it has nevertheless contributed effectively in obtaining reproducible and consistent performance and thus can be exploited to generate consistent voltage output.

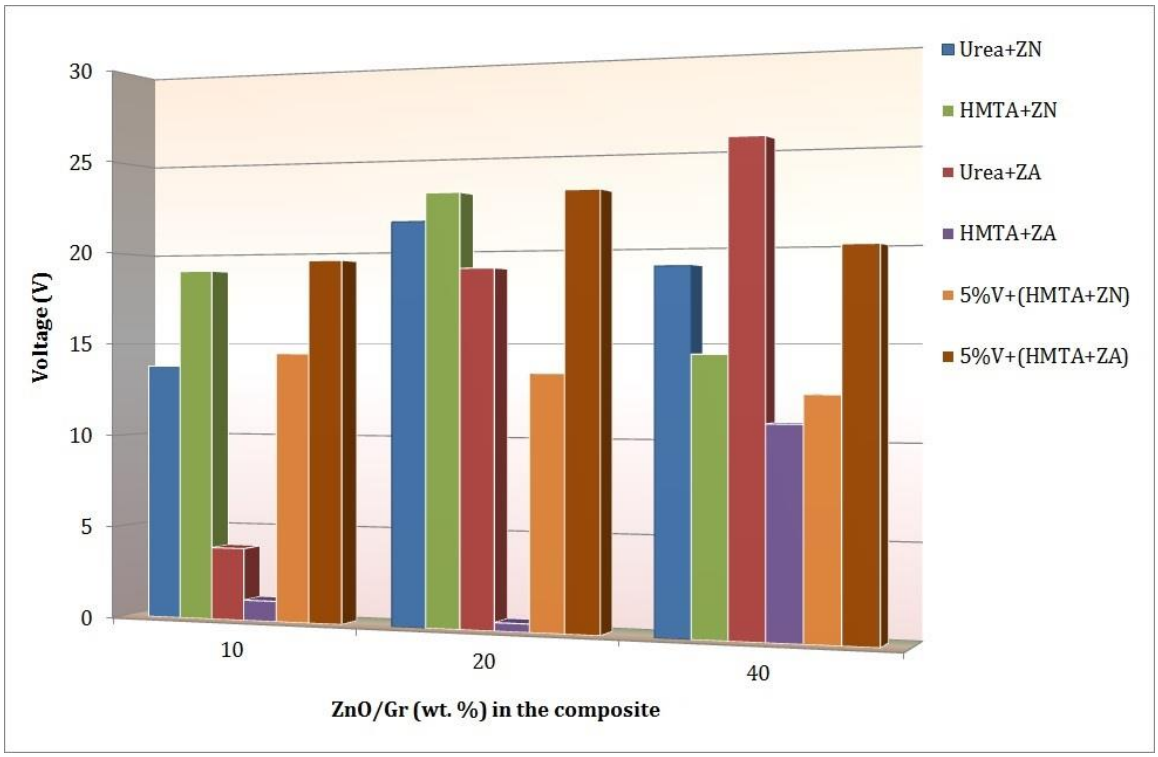

Figure 40: Comparison of open circuit voltage summary

The output voltage was nearly the same when the 40 wt.% (5 wt.% V_2O_5- ZnO/Gr)-PVDF was manually bent or simply pressed; this is shown in Fig. 41. The reproducibility of the open circuit voltage of a given sample in four bending/unbending experiments is evident from the results shown in Figure 42.

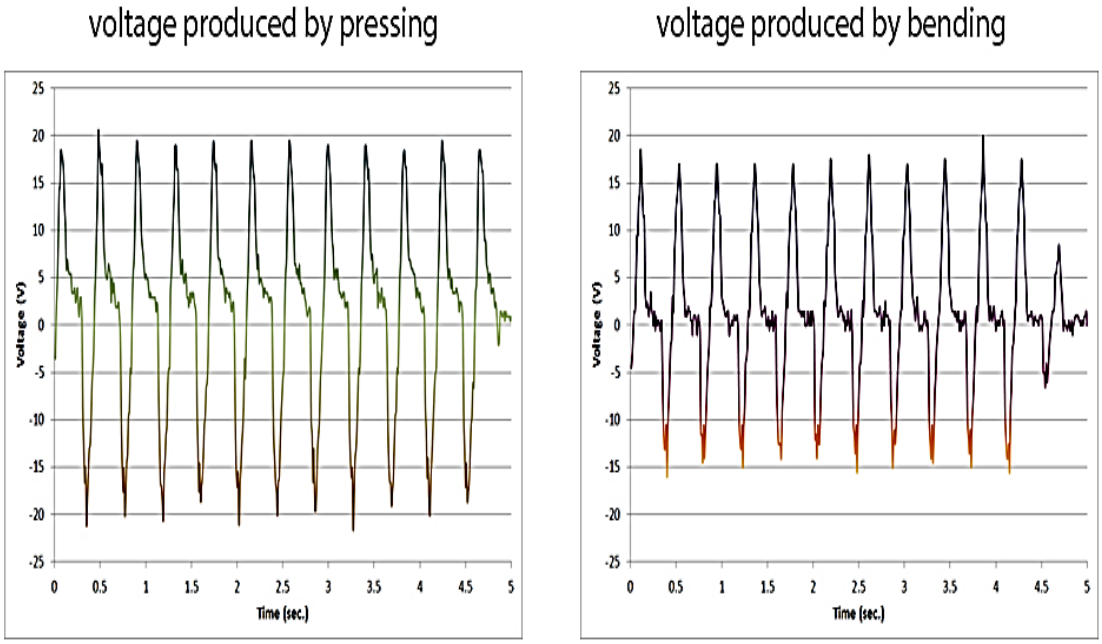

Figure 41: Output voltage generated upon pressing or bending the sample

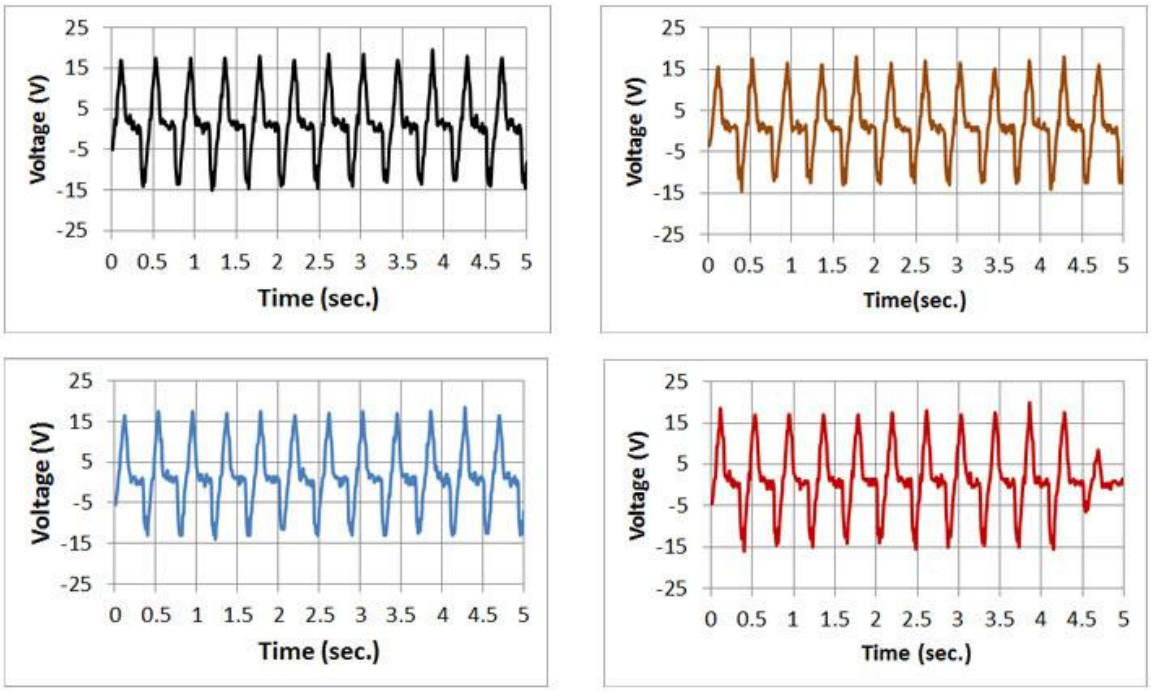

Figure 42: Reproducibility of the output voltage in different runs

Chapter 5

5.1. Conclusions

A systematic study had been conducted on the synthesis, characterization and fabrication, of piezoelectric ZnO-based composites for application as potential energy harvesting devices. The following conclusions could be drawn:

- ZnO-based composites were successfully synthesized using a simple preparative technique and inexpensive starting materials.
- Role of starting materials (zinc source and reducing agent) and additives was elucidated.
- The feasibility of incorporation of functional materials (such as, graphene and PVDF) was investigated.
- Fabrication of EHD device containing a piezoelectric ceramic (ZnO), graphene and PVDF with or without V_2O_5 was investigated.
- Generation of voltages by mere bending and pressing holds promise of using these devices in various applications.

5.2. Recommendations

Based on the promising results that have been achieved in this work, following recommendations are made for future work:

- Investigating the effect of lower loading of V_2O_5 (< 2.5 wt. %) and the role of other additives that do not disrupt the hexagonal rod morphology of ZnO upon incorporation.
- Investigating the effect of vibration and frequency variation on the output voltage of ZnO-based nanocomposites.
- Exploring the application of ZnO-based nanocomposites in other applications, such as gas sensing.
- Investigating the perovskite-structured $ZnMO_3$ (M = Ti or Sn) and their composites for the possibility of using as alternative energy harvesting devices.

References

[1] Yang X, Kong X, Tan S, Li G, Ling W, Z. E., Spatially-confined Crystallization of Poly(vinylidene Fluoride), *Polymer International,* **49** (2000), 1525-1528.

[2] B. Kumar, K.Y. Lee, H.-K. Park, S.J. Chae, Y.H. Lee, S.-W. Kim, Controlled growth of semiconducting nanowire, nanowall, and hybrid nanostructures on graphene for piezoelectric nanogenerators, *Acs Nano,* **5** (2011), 4197-4204.

[3] M.M. Seabaugh, G.L. Cheney, K. Hasinska, A.-M. Azad, E.M. Sabolsky, S.L. Swartz, W.J. Dawson, Development of a templated grain growth system for texturing piezoelectric ceramics, *Journal of intelligent material systems and structures,* **15** (2004), 209-214.

[4] B. Kumar, S.-W. Kim, Energy harvesting based on semiconducting piezoelectric ZnO nanostructures, *Nano Energy,* **1** (2012), 342-355.

[5] K.I. Park, M. Lee, Y. Liu, S. Moon, G.T. Hwang, G. Zhu, J.E. Kim, S.O. Kim, K. Kim do, Z.L. Wang, K.J. Lee, Flexible nanocomposite generator made of BaTiO(3) nanoparticles and graphitic carbon, *Advanced materials,* **24** (2012), 2999-3004, 2937.

[6] J. Chang, M. Dommer, C. Chang, L. Lin, Piezoelectric nanofibers for energy scavenging applications, *Nano Energy,* **1** (2012), 356-371.

[7] Z.L. Wang, J. Song, Piezoelectric nanogenerators based on zinc oxide nanowire arrays, *Science,* **312** (2006), 242-246.

[8] X. Wang, Piezoelectric nanogenerators—Harvesting ambient mechanical energy at the nanometer scale, *Nano Energy,* **1** (2012), 13-24.

[9] M.Y. Soomro, I. Hussain, N. Bano, O. Nur, M. Willander, Piezoelectric power generation from zinc oxide nanowires grown on paper substrate, *physica status solidi (RRL) - Rapid Research Letters,* **6** (2012), 80-82.

[10] R. Yang, Y. Qin, L. Dai, Z.L. Wang, Power generation with laterally packaged piezoelectric fine wires, *Nature Nanotechnology,* **4** (2008), 34-39.

[11] M.H.M. Ramli, M.H.M. Yunus, C.Y. Low, A. Jaffar, Scavenging Energy from Human Activities Using Piezoelectric Material, *Procedia Technology,* **15** (2014), 828-832.

[12] R.H. Kinner, *Green Energy Through Smart Ceramics*, MS Thesis ,The University of Toledo, 2011.

[13] R. Kinner, A.-M. Azad, G. Srinivasan, G. Sreenivasulu, M. Jain, ZnO/LSMO Nanocomposites for Energy Harvesting, *Smart Nanosystems in Engineering and Medicine,* **2** (2012), 15.

[14] 'Global piezoelectric device market', Acmite market intelligence, (2015) <http://www.acmite.com/market-reports/materials/global-piezoelectric-device-market-report.html> [Accessed 09, February, 2015 2014].

[15] B. Jaleh, A. Jabbari, Evaluation of reduced graphene oxide/ZnO effect on properties of PVDF nanocomposite films, *Applied Surface Science,* **320** (2014), 339-347.

[16] This Month In Physics History "March 1880: The Curie Brothers Discover Piezoelectricity", *APS News,* **23** (2014), 2-3.

[17] J. Curie, P. Curie, "Development via compression of electric polarization in hemihedral crystals with inclined faces ", *Bulletin de la Societe de Minerologique de France,* **3** (1880), 90-93.

[18] J. Curie, P. Curie, "Contractions and expansions produced by voltages in hemihedral crystals with inclined faces", *Comptes Rendus,* **93** (1881), 1137-1140.

[19] G. Lippman, "Principal of the conservation of electricity", *Annales de Chemie et de Physique* **24** (1881), 145.

[20] C.M. Chilowsky, M.P. Langévin, Procídés et appareil pour production de signaux sous-marins dirigés et pour la localsation à distances d'obstacles sons-marins., < 502913> (1916).

[21] Ü. Özgür, Y.I. Alivov, C. Liu, A. Teke, M.A. Reshchikov, S. Doğan, V. Avrutin, S.-J. Cho, H. Morkoç, A comprehensive review of ZnO materials and devices, *Journal of Applied Physics,* **98** (2005), 041301.

[22] Z.L. Wang, ZnO nanowire and nanobelt platform for nanotechnology, *Materials Science and Engineering: R: Reports,* **64** (2009), 33-71.

[23] A. Onodera, M. Takesada, Electronic Ferroelectricity in II-VI Semiconductor ZnO, Advances in Ferroelectrics, 2012.

[24] K. S. Novoselov, A. K. Geim, S. V. Morozov et al., Electric field in atomically thin carbon films *Science* **306** (2004), 666-669.

[25] D.R. Cooper, B. D'Anjou, N. Ghattamaneni, B. Harack, M. Hilke, A. Horth, N. Majlis, M. Massicotte, L. Vandsburger, E. Whiteway, V. Yu, Experimental Review of Graphene, *ISRN Condensed Matter Physics,* **2012** (2012), 1-56.

[26] K.u. Hasan, *Graphene and ZnO Nanostructures forNano-Optoelectronic & Biosensing Applications*, 2012.

[27] H.-J. Shin, W.M. Choi, D. Choi, G.H. Han, S.-M. Yoon, H.-K. Park, S.-W. Kim, Y.W. Jin, S.Y. Lee, J.M. Kim, Control of electronic structure of graphene by various dopants and their effects on a nanogenerator, *Journal of the American Chemical Society,* **132** (2010), 15603-15609.

[28] H.M. Correia, M. Ramos, Modelling molecular transformations in ferroelectric polymers induced by mechanical and electrical means, *Ferroelectrics,* **338** (2006), 179-184.

[29] S. Sharma, Ferrolectric nanofibers: principle, processing and applications, *Adv. Mat. Lett.,* **4** (2013), 522-533.

[30] M. Lee, C.-Y. Chen, S. Wang, S.N. Cha, Y.J. Park, J.M. Kim, L.-J. Chou, Z.L. Wang, A Hybrid Piezoelectric Structure for Wearable Nanogenerators, *Advanced materials,* **24** (2012), 1759-1764.

[31] 'Crystallinity in polymers, crystalline and amorphous polymers', University of Cambridge, (2015) <http://www.doitpoms.ac.uk/tlplib/polymers/crystalline.php> [Accessed 11,March 2015].

[32] A.R. Hutson, Piezoelectricity and Conductivity in ZnO and CdS, *Physical Review Letters,* **4** (1960), 505-507.

[33] F.S. Hickernell, Zinc-oxide thin-film surface-wave transducers, *Proceedings of the IEEE,* **64** (1976), 631-635.

[34] J. Briscoe, M. Stewart, M. Vopson, M. Cain, P.M. Weaver, S. Dunn, Nanostructured p-n Junctions for Kinetic-to-Electrical Energy Conversion, *Advanced Energy Materials,* **2** (2012), 1261-1268.

[35] M. Lee, J. Bae, J. Lee, C.-S. Lee, S. Hong, Z.L. Wang, Self-powered environmental sensor system driven by nanogenerators, *Energy & Environmental Science,* **4** (2011), 3359.

[36] G. Zhu, R. Yang, S. Wang, Z.L. Wang, Flexible high-output nanogenerator based on lateral ZnO nanowire array, *Nano Lett,* **10** (2010), 3151-3155.

[37] Y. Hu, Y. Zhang, C. Xu, L. Lin, R.L. Snyder, Z.L. Wang, Self-powered system with wireless data transmission, *Nano Lett,* **11** (2011), 2572-2577.

[38] E.S. Nour, A. Khan, O. Nur, M. Willander, A Flexible Sandwich Nanogenerator for Harvesting Piezoelectric Potential from Single Crystalline Zinc Oxide Nanowires, *Nanomaterials and Nanotechnology* (2014), 1.

[39] L.N. Dem'Yanets, L.E. Li, T.G. Uvarova, Zinc oxide: Hydrothermal growth of nano- and bulk crystals and their luminescent properties, *J. Mater. Sci.,* **41** (2006), 1439-1444.

[40] M. Singhal, V. Chhabra, P. Kang, D.O. Shah, Synthesis of ZnO nanoparticles for varistor application using Zn-substituted Aerosol OT microemulsion, *Mater. Res. Bull.,* **32** (1997), 239-247.

[41] I.U. Haq, A.-M. Azad, Experimental Artifacts for Morphological Tweaking of Chemical Sensor Materials: Studies on ZnO, *sensors,* **12** (2012), 8259-8277.

[42] R. Joshi, P. Kumar, A. Gaur, K. Asokan, Structural, optical and ferroelectric properties of V doped ZnO, *Applied Nanoscience,* **4** (2013), 531-536.

[43] Y.C. Yang, C. Song, X.H. Wang, F. Zeng, F. Pan, Giant piezoelectric d33 coefficient in ferroelectric vanadium doped ZnO films, *Applied Physics Letters,* **92** (2008), 012907.

[44] Y.J. Xing, Z.H. Xi, Z.Q. Xue, X.D. Zhang, J.H. Song, R.M. Wang, J. Xu, Y. Song, S.L. Zhang, D.P. Yu, Optical properties of the ZnO nanotubes synthesized via vapor phase growth, *Applied Physics Letters,* **83** (2003), 4.

[45] Z.L. Wang, Zinc oxide nanostructures: growth, properties and applications, *Journal of Physics: Condensed Matter,* **16** (2004), R829.

[46] W.Z. Xu, Z.Z. Ye, D.W. Ma, H.M. Lu, L.P. Zhu, B.H. Zhao, X.D. Yang, Z.Y. Xu, Quasi-aligned ZnO nanotubes grown on Si substrates, *Applied Physics Letters,* **87** (2005), 093110.

[47] G.-W. She, X.-H. Zhang, W.-S. Shi, X. Fan, J.C. Chang, C.-S. Lee, S.-T. Lee, C.-H. Liu, Controlled synthesis of oriented single-crystal ZnO nanotube arrays on transparent conductive substrates, *Applied Physics Letters,* **92** (2008), 053111.

[48] A. Wei, L. Pan, W. Huang, Recent progress in the ZnO nanostructure-based sensors, *Materials Science and Engineering: B,* **176** (2011), 1409-1421.

[49] G. She, X. Zhang, W. Shi, X. Fan, J. Chang, Electrochemical/chemical synthesis of highly-oriented single-crystal ZnO nanotube arrays on transparent conductive substrates, *Electrochemistry Communications,* **9** (2007), 2784-2788.

[50] S. Xu, Z.L. Wang, One-dimensional ZnO nanostructures: Solution growth and functional properties, *Nano Research,* **4** (2011), 1013-1098.

[51] Y. Chen, X. Zheng, X. Feng, The fabrication of vanadium-doped ZnO piezoelectric nanofiber by electrospinning, *Nanotechnology,* **21** (2010), 055708.

[52] H. Saeki, H. Tabata, T. Kawai, Magnetic and electric properties of vanadium doped ZnO films, *Solid State Communications,* **120** (2001), 439-443.

Vitae

Name	Khalid Hayder Abdalla Elkhider
Nationality	Sudanese
Date of Birth	1985/2/22
Email	khalidhayder@kfupm.edu.sa, khalid_h_2001@hotmail.com
Address	KFUPM campus, Dhahran
Academic Background	Mr. Khalid H. Abdalla is a Master student in King Fahd University in chemical engineering department and also a Research Assistant in Center of Nanotechnology. He joined the CENT in 2012 and his research interest area is in catalysis, synthesis, characterization, and applications of metal oxides. He graduated from University of Gezira as a chemical engineer with first class degree (Honor) in 2009.